information services
gwasanaethau gwybodaeth

[]

Highlights

A novel mathematical model of AIDS-associated Kaposi sarcoma: analysis and optimal control

RF Kaondera-Shava,E Lungu,B Szomolay

- A new mathematical model of AIDS-associated Kaposi sarcoma is presented which incorporates the effect of viral loads in the proliferation terms of the immune cell populations

- We distinguish between weak and strong viral source terms – the latter accounting for non-adherence to HAART for example. These scenarios are able to capture and predict potential outcomes of AIDS-KS

- Rigorous stability analysis and optimal control analysis is presented; the latter shows that combined antiretroviral therapy is able to remove the viral reservoirs efficiently

- The results suggest early treatment for HIV-1 in order to maintain low viral load and hence preventing AIDS-related KS

A novel mathematical model of AIDS-associated Kaposi sarcoma: analysis and optimal control

RF Kaondera-Shava[a,*], E Lungu[a] and B Szomolay[b]

[a]*Department of Mathematics and Statistical Sciences, Botswana International University of Science and Technology, Private Bag 16, Palapye, Botswana*

[b]*Systems Immunity Research Institute, Cardiff University School of Medicine, Cardiff, CF14 4XN United Kingdom*

ARTICLE INFO

Keywords:
Kaposi sarcoma
cART
optimal control
viral load
HIV
KSHV

ABSTRACT

Kaposi sarcoma (KS) has been the most common HHV-8 virus-induced neoplasm associated with HIV infection. Although the standard KS therapy has not changed in 20 years, not all cases of KS will respond to the same therapy. The goal of current AIDS-KS treatment modalities is to reconstitute the immune system and suppress HIV-1 replication, but newer treatment modalities are on horizon. There are very few mathematical models that have included HIV-1 viral load (VL) measures, despite VL being a key determinant of treatment outcome. Here we introduce a mathematical model that consolidates the effect of both HIV-1 and HHV-8 VL on KS tumor progression by incorporating low or high VLs into the proliferation terms of the immune cell populations. Regulation of HIV-1/HHV-8 VL and viral reservoir cells is crucial for restoring a patient to an asymptomatic stage. Therefore, an optimal control strategy given by a combined antiretroviral therapy (cART) is derived. The results indicate that the drug treatment strategies are capable of removing the viral reservoirs faster and consequently, the HIV and KS tumor burden is reduced. The predictions of the mathematical model have the potential to offer more effective therapeutic interventions based on viral and virus-infected cell load and support new studies addressing the superiority of VL over CD4 cell count in HIV pathogenesis.

1. Introduction

Kaposi sarcoma (KS) is a cancer caused Human herpesvirus-8 (HHV-8), also known as Kaposi's sarcoma-associated herpes virus (KSHV), a virus which is usually transmitted sexually, via blood transfusion, organ transplant or saliva [38, 46]. Appearance of the cancer can be in several parts or a specific part of the body [43]. KS remains the most common cancer in sub-Sahara Africa and the second most common cancer in HIV-infected patients worldwide [26]. Infection with HIV afflicts approximately 37.9 million people worldwide (end 2018) [47] and results in impaired immune responses which may affect defenses against pathogens [48]. Consequently, the highest risk group to acquire KS is patients with suppressed immune systems [7, 23]. Despite the introduction of highly active antiretroviral therapy (HAART), KS still continues to be diagnosed in HIV-infected patients [7]. The distribution of KS is concentrated in sub-Sahara Africa where the heaviest burden of HIV-AIDS is concentrated [7, 26]. Since HIV is an immunosuppressive virus, it promotes the development of KS in individuals dually infected with both viruses, HIV-1 and HHV-8, a combination which has proved to be fatal [26].

This cancer became more widely known as one of the AIDS defining illnesses in the 1980s when it appeared in young gay men in America [7, 10, 13]. Chang *et al.* [6] identified the herpesvirus-like DNA sequences in AIDS-KS. This study [6] as well as other studies for example [44] showed that AIDS-KS depends upon prior infection to HHV-8. In competent immune systems, however, acquisition of HHV-8 does not necessarily guarantee the development of KS, as many people can remain latently infected with HHV-8 throughout their entire life without developing clinical symptoms [14]. Foreman's review article [13] supported the suggestion that HIV-1 virions play an important role in the development of KS tumor cells by activating latently infected B-cells which rapture leading to the increase in the HHV-8 VL.

If the VL is high, T-helper cells tend to be destroyed more quickly. Therefore, the aim of antiretroviral treatment is to keep the VL as low as possible. As recommended by the World Health Organization (WHO) [34], VL is the preferred monitoring approach to diagnose and confirm HAART treatment failure. WHO [32] has recommended a threshold

---

*Corresponding author

✉ roseshava@gmail.com (R. Kaondera-Shava); lungue@biust.ac.bw (E. Lungu); szomolayb@cardiff.ac.uk (B. Szomolay)
ORCID(s):

of 100 HIV-1 copies/mL above which an individual must receive ART treatment. Chiereghin *et al.* [8] indicated a threshold of 500 HHV-8 copies/mL. Despite the recommendation to use VL over CD4 cell count when predicting HIV transmission and pathogenesis, in the past 20 years only 6% of studies related to HIV simulation included consideration of VL or VL testing [15]. This is surprising, even though the superiority of VL over CD4 cell count in HIV progression on patients receiving ART has been shown mathematically [40].

Although HHV-8 seroprevalence is relatively low in Western countries and Asia, but it is as high as 50% in sub-Saharan Africa and even higher in HIV positive individuals [51], thus representing a potentially large population that can develop KS. Nevertheless, only a very few KS mathematical models describing within-host dynamics have been published. The few examples include the mathematical models by Nani and Jin [30, 31] and Szomolay and Lungu [44]. The study of Nani and Jin's [30, 31] describes the dynamics of AIDS-KS during HAART, concluding that both HAART and adoptive immunotherapy are necessary to annihilate both HIV and KS. The framework developed by Szomolay and Lungu [44] included the adaptive immune system and the effect of adhering to cART therapy. Their findings established that adherence to treatment has a significant impact on the prognosis of KS.

Using mathematical modelling, we study a dynamic model in Figure 1 comprising of the interactions between infected B and CD4$^+$ T-cells, KS cells, HIV-1 and HHV-8 virions and virus-specific effector cells. The model consolidates the effect of low and high VL in the proliferation terms of the infected cells and virus-specific effector cells. Denoting x_6 the HIV-1 VL and x_7 the HHV-8 VL, we define a weak viral source model ($H_1(x_6, \beta) = x_6^\beta$ and $H_8(x_7, \gamma) = x_7^\gamma$) and a strong viral source model ($H_1(x_6, \beta) = x_6^\beta + x_6$ and $H_8(x_7, \gamma) = x_7^\gamma + x_7$) by incorporating the H_1, H_8 functions into the proliferation terms of immune cells. By considering different parameter scenarios for $0 \leq \beta, \gamma \leq 1$, we show that the two models can correctly predict the pathogenesis of AIDS-KS. We apply optimal control to the model with weak viral source and determine the efficacy levels for cART (HAART plus KS therapy) that minimize the KS cell and infected CD4$^+$ T-cell burden and the associated costs. The conclusions will be the same for the model with strong viral source.

The paper is organized as follows: In Section 2, we propose the model with weak viral source which describes the interactions between the KS tumor cells and components of the immune system in the presence of HIV-1 and HHV-8 infection. The model analysis is given in Section 3 which deals with the local and global stability of equilibrium points for the model and we discuss the biological meanings of these steady states. This is followed by a sensitivity analysis of the parameters with respect to the reproduction numbers in Section 4. Numerical results without optimal control are presented in Section 5. In Section 6 we consider the model with strong viral source due to non-adherence to medication, additionally, numerical simulations are also presented. Optimal control methods are considered in Section 7 and finally, some concluding remarks follow in Section 8.

2. Weak Viral Source Model with $H_1(x_6, \beta) = x_6^\beta$ and $H_8(x_7, \gamma) = x_7^\gamma$

We construct a mathematical model describing the dynamics of viruses and associated immune cells as defined in Figure 1. Denote x_1, x_2, x_3, x_4, x_5, x_6, x_7 the infected B-cells, KS cells, HIV-1-specific effector cells, infected CD4$^+$ T-cells, HHV-8-specific effector cells, HIV-1 VL and HHV-8 VL, respectively. The proliferation terms in the equations of the infected cells and effector cells will be of the type $H_1(x_6, \beta) = x_6^\beta$ and $H_8(x_7, \gamma) = x_7^\gamma$, where the magnitude of proliferation is expressed by $0 \leq \beta \leq 1$ for HIV-1 and $0 \leq \gamma \leq 1$ for HHV-8 VLs.

Infected B-cell dynamics:

$$\dot{x}_1 \quad = r_{x_1} H_8(x_7, \gamma) - \mu_{x_1} x_1 - \kappa_1 x_1 x_5 \tag{1}$$

Equation (1) describes the rate of change of actively infected B-cells, x_1. In this model we have ignored the class of latently infected B-cells. The actively infected B-cells are generated by infection of susceptible B-cells by HHV-8 as well as proliferation of infected B-cells. We account for these two mechanisms through the first term. The second and third terms describe the loss due to lytic death and the killing of infected B-cells by HHV-8-specific effector cells.

KS cell dynamics:

$$\dot{x}_2 \quad = \quad (1 - \eta_c)\alpha x_1 \left(1 - \frac{x_2}{\omega}\right) - \kappa_3 x_2 x_5 \tag{2}$$

Equation (2) describes the rate of change of KS cells, x_2. The first term assumes logistic growth for these cells [49, 17] and the second term represents the killing of KS cells by HHV-8-specific effector cells. The growth of this population is dependent on the population of infected B-cells, x_1, but it is self-regulated. When the KS population

Table 1
Model variables and parameters.

Symbols	Description
x_1	density of infected B-cells
x_3	density of HIV-1 specific effector cells
x_5	density of HHV-8 specific effector cells
x_4	density of infected CD4$^+$ T-cells
x_2	density of KS cells
x_6	density of HIV-1 virions
x_7	density of HHV-8 virions
s_{x_3}, s_{x_5}	source of virus-specific effector cells
r_{x_1}	growth rate of infected B-cells
r_{x_4}	growth rate of infected CD4$^+$ T-cells
r_{x_3}, r_{x_5}	growth rate of virus specific effector cells
ω	maximum carrying capacity of KS cells
κ_1	lysis of infected B-cells
κ_3	lysis of infected KS cells
κ_4	lysis of infected CD4$^+$ T-cells
μ_{x_1}	lytic death of infected B-cells
μ_{x_3}, μ_{x_5}	natural death of virus specific effector cells
μ_{x_4}	lytic death of infected CD4$^+$ T-cells
μ_{x_6}	natural death of HIV-1 virions
μ_{x_7}	natural death of HHV-8 virions
α	growth rate of KS cells
δ	proliferation rate of HIV-1 virions
N_{x_6}	maximum carying capacity of infected CD4$^+$ T-cells
N_{x_7}	maximum carying capacity of infected B-cells
η_c	efficacy of KS therapy
ζ_p	efficacy of PIs
ζ_r	efficacy of RTIs

increases towards the carrying capacity, ω, the cancer goes into remission. This can be also achieved due to KS therapy, expressed by the efficacy function ($0 \leq \eta_c \leq 1$).

HIV-1 specific effector cells dynamics:

$$\dot{x_3} = s_{x_3} + r_{x_3} x_3 H_1(x_6, \beta) - \mu_{x_3} x_3 \tag{3}$$

The dynamics of HIV-1 specific effector cells is given by Equation (3). The first two terms represent the constant source of the effector cells and the proliferation due to the presence of HIV-1, respectively. The third term accounts for natural death.

Infected CD4$^+$ T-cells dynamics:

$$\dot{x_4} = (1 - \zeta_r) r_{x_4} H_1(x_6, \beta) - \kappa_4 x_3 x_4 - \mu_{x_4} x_4 \tag{4}$$

Equation (4) describes the rate of change of infected CD4$^+$ T-cells, x_4. This population increases by infection of healthy CD4$^+$ T-cells by HIV-1 and proliferation. These two sources are represented by the first term which is assumed to depend on the density of HIV-1, x_6. The second term accounts for the killing of infected cells by HIV-1 specific effector cells. The infected cells are lysed at a rate of μ_{x_4} due to which new HIV-1 particles are produced. The efficacy function ζ_r represents the effect of reverse transcriptase inhibitors (RTIs)that are a component of HAART therapy.

HHV-8 specific effector cells dynamics:

$$\dot{x_5} = s_{x_5} + r_{x_5} x_5 H_8(x_7, \gamma) - \mu_{x_5} x_5 \tag{5}$$

The HHV-8-specific effector cells are replenished at a constant rate s_{x_5}, undergo proliferation in the presence of HHV-8 and are lost due to natural death.
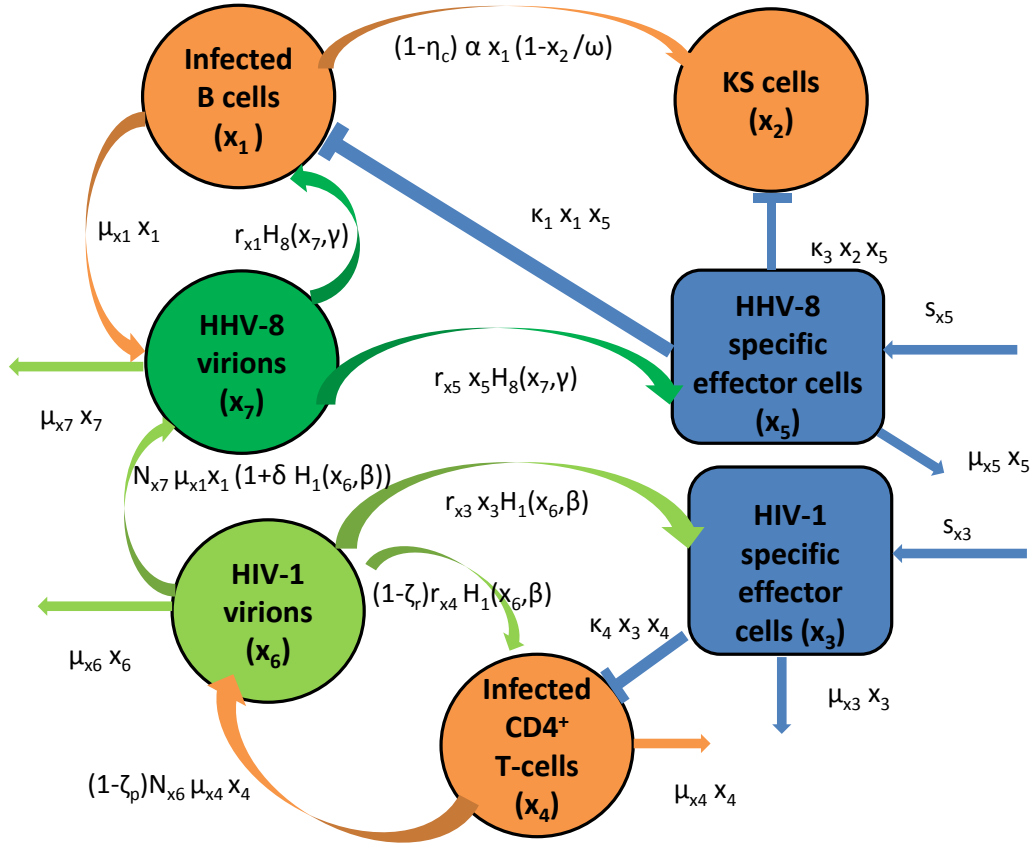
Figure 1: Schematic presentation of the mathematical model showing the interactions between KS and the immune cells in the presence of HIV-1 and HHV-8. Blocked arrows indicate killing of infected cells by the effector cells and sharp arrows indicate interaction.

HIV-1 dynamics:

$$\dot{x}_6 = (1 - \zeta_p)N_{x_6}\mu_{x_4}x_4 - \mu_{x_6}x_6 \qquad (6)$$

Following Perelson and Nelson [36], the HIV-1 dynamics are governed by two processes: the first term describes the release of new free viral particles due to lytic death of infected CD4+ T-cells and the second term accounts to loss due to natural death. The efficacy function ζ_p represents the effect of protease inhibitors (PIs) that are a component of HAART therapy.

HHV-8 dynamics:

$$\dot{x}_7 = N_{x_7}\mu_{x_1}x_1(1 + \delta H_1(x_6, \beta)) - \mu_{x_7}x_7 \qquad (7)$$

The first term describes the production of free HHV-8 virions due to lysis of infected B-cells and their enhancement by HIV-1 at a rate δ. The last term accounts for loss due to natural death.

In what follows, we will assume there is no cART therapy (e.g. $\eta_c = \zeta_p = \zeta_r = 0$) and the effect of cART will be investigated using optimal control in Section 7. We now investigate how the infection characteristics are altered for the cases when $\gamma = \beta$ and when $\gamma \neq \beta$. More specifically, we consider three cases when the infection parameters (γ, β) are zero, which represents constant source terms for the infected and effector cell dynamics. Secondly, we consider the case when one infection parameter (for HHV-8) is zero, that is $\gamma = 0$, but the infection parameter for HIV-1 is non-zero, that is $\beta = 1$. Lastly, we consider the case when both infection parameters γ and β are nonzero. These cases are summarised as follows: (i) $\gamma = \beta = 0$, (ii) $\gamma = 0$ and $\beta = 1$, (iii) $\gamma = \beta = 1$.

3. Model Analysis

Here we will show local stability for (ii)-(iii) and global stability for (i)-(iii) of the equilibrium points and describe the parameter choices. Throughout this paper it will be assumed that $\mu_{x_3} > r_{x_3}$ and $\mu_{x_5} > r_{x_5}$ and M_{ij} for $i, j = 1 \ldots 7$ will denote matrix entries of $\mathbf{M}$ defined in A.1.

3.1. Virus Free Equilibrium (VFE) $\mathcal{E}_0$ for $\gamma = \beta = 0$

In case when all cell populations have constant source terms, the VFE, for which

$$x_1 = x_2 = x_4 = x_6 = x_7 = 0 \implies r_{x_1} = r_{x_4} = 0 \tag{8}$$

is given by

$$\mathcal{E}_0 = (0, 0, \overset{*}{x_3}, 0, \overset{*}{x_5}, 0, 0) \text{ where } \overset{*}{x_3} = \frac{s_{x_3}}{(\mu_{x_3} - r_{x_3})} > 0, \ \overset{*}{x_5} = \frac{s_{x_5}}{(\mu_{x_5} - r_{x_5})} > 0, \ \mu_{x_3} > r_{x_3}, \ \mu_{x_5} > r_{x_5}.$$

The equilibrium point $\mathcal{E}_0$ is locally stable and $\mathcal{R}_0 = 0$.

3.2. Stability Analysis of VFE $\mathcal{E}_0$

For the case (i)-(iii), the system (1)–(7) can be rewritten in matrix form as $\dot{x} = \mathbf{A}x^\gamma + \mathbf{B}x$ where the matrices $\mathbf{A}$ and $\mathbf{B}$ are given below:

$$\mathbf{A} = \begin{pmatrix} 0 & 0 & 0 & 0 & 0 & 0 & M_{17} \\ 0 & 0 & 0 & 0 & 0 & 0 & 0 \\ 0 & 0 & 0 & 0 & 0 & M_{36} & 0 \\ 0 & 0 & 0 & 0 & 0 & M_{46} & 0 \\ 0 & 0 & 0 & 0 & 0 & 0 & M_{57} \\ 0 & 0 & 0 & 0 & 0 & 0 & 0 \\ 0 & 0 & 0 & 0 & 0 & 0 & 0 \end{pmatrix}, \quad \mathbf{B} = \begin{pmatrix} M_{11} & 0 & 0 & 0 & 0 & 0 & 0 \\ M_{21} & M_{22} & 0 & 0 & 0 & 0 & 0 \\ 0 & 0 & M_{33} & 0 & 0 & 0 & 0 \\ 0 & 0 & 0 & M_{44} & 0 & 0 & 0 \\ 0 & 0 & 0 & 0 & M_{55} & 0 & 0 \\ 0 & 0 & 0 & M_{64} & 0 & M_{66} & 0 \\ \frac{M_{71}}{1+\delta} & 0 & 0 & 0 & 0 & 0 & M_{77} \end{pmatrix} \tag{9}$$

3.2.1. Stability Analysis Case (ii)

Consider the case of HIV-1-dependent and HHV-8-independent proliferation terms ($\gamma = 0$ and $\beta = 1$). The system (1)–(7) reduces to $\dot{x} = \mathbf{H}x$, where $\mathbf{H}$ is given by

$$\mathbf{H} = \begin{pmatrix} M_{11} & 0 & 0 & 0 & 0 & 0 & 0 \\ M_{21} & M_{22} & 0 & 0 & 0 & 0 & 0 \\ 0 & 0 & M_{33} & 0 & 0 & M_{36} & 0 \\ 0 & 0 & 0 & M_{44} & 0 & M_{46} & 0 \\ 0 & 0 & 0 & 0 & M_{55} & 0 & 0 \\ 0 & 0 & 0 & M_{64} & 0 & M_{66} & 0 \\ \frac{M_{71}}{1+\delta} & 0 & 0 & 0 & 0 & 0 & M_{77} \end{pmatrix} \tag{10}$$

The matrix $\mathbf{H}$ has five negative eigenvalues:

$$\lambda_1 = -\mu_{x_3}, \ \lambda_2 = -(\mu_{x_5} - r_{x_5}), \ \lambda_3 = -\kappa_3 \frac{s_{x_5}}{(\mu_{x_5} - r_{x_5})}, \ \lambda_4 = -\mu_{x_7}, \ \lambda_5 = -\left(\mu_{x_1} + \kappa_1 \frac{s_{x_5}}{(\mu_{x_5} - r_{x_5})}\right).$$

The remaining two are obtained from the characteristic polynomial $P(\lambda) = \lambda^2 + a_1 \lambda + a_2$, where

$$a_1 = \left[\left(\mu_{x_4} + \kappa_4 \frac{s_{x_3}}{(\mu_{x_3} - r_{x_3})}\right) + \mu_{x_6}\right] > 0, \quad a_2 = \left[\frac{\mu_{x_6}}{(\mu_{x_3} - r_{x_3})}[\mu_{x_4}(\mu_{x_3} - r_{x_3}) + \kappa_4 s_{x_3}]\right](1 - \mathcal{R}_0) > 0$$

for $\mathcal{R}_0 = \frac{r_{x_4} N_{x_6} \mu_{x_4}(\mu_{x_3} - r_{x_3})}{[\kappa_4 s_{x_3} + \mu_{x_4}(\mu_{x_3} - r_{x_3})]\mu_{x_6}} < 1$. The stability results are summarised in the following theorem:

Theorem 1. *For $\gamma = 0$ and $\beta = 1$ the VFE, $\mathcal{E}_0$, for the system (1)–(7) is stable if $\mathcal{R}_0 < 1$.*

3.2.2. Stability Analysis Case (iii)

Consider the case of HIV-1- and HHV-8-dependent proliferation terms ($\gamma = \beta = 1$.) Then system (1)–(7) can be written as $\dot{x} = \mathbf{C}x$, where $\mathbf{C} = \mathbf{A} + \mathbf{B}$ is given by

$$\mathbf{C} = \begin{pmatrix} M_{11} & 0 & 0 & 0 & 0 & 0 & M_{17} \\ M_{21} & M_{22} & 0 & 0 & 0 & 0 & 0 \\ 0 & 0 & M_{33} & 0 & 0 & M_{63} & 0 \\ 0 & 0 & 0 & M_{44} & 0 & M_{64} & 0 \\ 0 & 0 & 0 & 0 & M_{55} & 0 & M_{57} \\ 0 & 0 & 0 & M_{64} & 0 & M_{66} & 0 \\ \frac{M_{71}}{1+\delta} & 0 & 0 & 0 & 0 & 0 & M_{77} \end{pmatrix} \tag{11}$$

Three of the eigenvalues of the matrix $\mathbf{C}$ are as follows: $\lambda_1 = -\mu_{x_3}$, $\lambda_2 = -\mu_{x_5}$ and $\lambda_3 = -\kappa_3 \dfrac{s_{x_5}}{(\mu_{x_5} - r_{x_5})}$. The other four eigenvalues are determined using the Routh-Hurwitz criterion from the characteristic polynomial $P(\lambda) = \lambda^4 + \sum\limits_{j=1}^{3} a_j \lambda^{4-j}$. Define

$$\mathcal{R}_{0x_6} = \frac{r_{x_4} N_{x_6} \mu_{x_4}(\mu_{x_3} - r_{x_3})}{\left[\kappa_4 s_{x_3} + \mu_{x_4}(\mu_{x_3} - r_{x_3})\right]\mu_{x_6}}, \qquad \mathcal{R}_{0x_7} = \frac{r_{x_1} N_{x_7} \mu_{x_1}(\mu_{x_5} - r_{x_5})}{\left[\kappa_1 s_{x_5} + \mu_{x_1}(\mu_{x_5} - r_{x_5})\right]\mu_{x_7}}, \qquad \mathcal{R}_{0x_i} = \text{Max}[\mathcal{R}_{0x_6}, \mathcal{R}_{0x_7}]$$

Then, if $\mathcal{R}_{0x_i} < 1$, it is easy to see that the coefficients of a_i for $i = 1, 2, 3, 4$ are all positive as shown in A.2. To conclude stability, it suffices to show that $a_1 a_2 a_3 - a_3^2 - a_1^2 a_4 > 0$. It is shown in A.3 that this condition is satisfied provided $\mu_{x_1} > 2\mu_{x_6}$ and $\mathcal{R}_{0x_i} < 1$. Our result is summarised as follows:

Theorem 2. For $\gamma = \beta = 1$ the VFE, $\mathcal{E}_0$, for the system (1)–(7) is stable if $\mathcal{R}_{0x_i} < 1$ and $\mu_{x_1} > 2\mu_{x_6}$.

3.2.3. Global Asymptotic Stability of VFE, $\mathcal{E}_0$

The global asymptotic stability (GAS) is established using the approach given in Castillo-Chavez *et al.* [5]. Define two classes: a class of non-infected states $W = (x_3, x_5)$ and a class of infected states $Z = (x_1, x_2, x_4, x_6, x_7)$. We rewrite the system (1)–(7) in the form of

$$\dot{W} = F(W, Z) \qquad \text{and} \qquad \dot{Z} = G(W, Z)$$

such that $G(W, \hat{0}) = \hat{0}, \hat{0} = (0, 0, 0, 0, 0)$, $W \in \mathbb{R}^2$ and $Z \in \mathbb{R}^5$. The functions $F(W, Z)$ and $G(W, Z)$ denote classes of non-infected and infected states, respectively, where

$$F(W, Z) = \begin{pmatrix} s_{x_3} + r_{x_3} x_3 x_6^\gamma - \mu_{x_3} x_3 \\ s_{x_5} + r_{x_5} x_5 x_7^\gamma - \mu_{x_5} x_5 \end{pmatrix}, \qquad G(W, Z) = \begin{pmatrix} r_{x_1} x_7^\gamma - \mu_{x_1} x_1 - \kappa_1 x_1 x_5 \\ \alpha x_1 \left(1 - \frac{x_2}{\omega}\right) - \kappa_3 x_2 x_5 \\ r_{x_4} x_6^\beta - \kappa_4 x_3 x_4 - \mu_{x_4} x_4 \\ N_{x_6} \mu_{x_4} x_4 - \mu_{x_6} x_6 \\ N_{x_7} \mu_{x_1}(1 + \delta x_6^\beta) x_1 - \mu_{x_7} x_7 \end{pmatrix}$$

We redefine the virus-free equillibrium as $\bar{\mathcal{E}}_0 = (W^*, \hat{0})$, where $W^* = \left(\dfrac{s_{x_3}}{(\mu_{x_3} - r_{x_3})}, \dfrac{s_{x_5}}{(\mu_{x_5} - r_{x_5})} \right)$. This theorem on GAS is proved in Castillo-Chavez *et al.* [5].

Theorem 3. (a) *The equillibrium point* $\bar{\mathcal{E}}_0 = (W^*, \hat{0})$ *is GAS for* $\gamma = \beta = 0$ *and* $\mathcal{R}_0 = 0$.

(b) *The equillibrium point $\bar{\mathcal{E}}_0 = (W^*, \hat{0})$ is GAS for $\gamma = 0$ and $\beta = 1$ if $\mathcal{R}_0 < 1$.*

(c) *The equillibrium point $\bar{\mathcal{E}}_0 = (W^*, \hat{0})$ is GAS for $\gamma = \beta = 1$ if $\mathcal{R}_{0x_i} < 1$.*

Proof. **3(a)**: The case $\gamma = \beta = 0$. Setting the infection variables of $F(W, Z)$ to zero, we have

$$F(W, 0) = (s_{x_3} - (\mu_{x_3} - r_{x_3})x_3, s_{x_5} - (\mu_{x_5} - r_{x_5})x_5)^T.$$

Consider the system

$$\dot{W} = s_x - \mu_x W, \quad W = \begin{pmatrix} x_3 \\ x_5 \end{pmatrix}, \quad \mu_x = \begin{pmatrix} \mu_{x_3} - r_{x_3} \\ \mu_{x_5} - r_{x_5} \end{pmatrix}, \quad s_x = \begin{pmatrix} s_{x_3} \\ s_{x_5} \end{pmatrix} \tag{12}$$

Then, the solution is given by

$$W(t) = \left(W(0) - \frac{s_x}{\mu_x} \right) e^{-\mu_x t} + \frac{s_x}{\mu_x}$$

Since $F(W, \hat{0})$ is a limiting function of $\dot{W} = F(W, Z)$, that is $\lim_{t \to \infty} W(t) = \left(\frac{s_{x_3}}{(\mu_{x_3} - r_{x_3})}, \frac{s_{x_5}}{(\mu_{x_5} - r_{x_5})} \right)^T = W^*$,

then $F(W^*, \hat{0})$ is GAS.

Let $y_3 = s_{x_3} - (\mu_{x_3} - r_{x_3})x_3$ and $y_5 = s_{x_5} - (\mu_{x_5} - r_{x_5})x_5$. Then F(W, $\hat{0}$) can be written as

$$\begin{pmatrix} \dot{y}_3 \\ \dot{y}_5 \end{pmatrix} = \begin{pmatrix} -\dfrac{1}{(\mu_{x_3} - r_{x_3})} & 0 \\ 0 & -\dfrac{1}{(\mu_{x_5} - r_{x_5})} \end{pmatrix} \begin{pmatrix} y_3 \\ y_5 \end{pmatrix},$$

where the eigenvalues are $\lambda_3 = -\dfrac{1}{(\mu_{x_3} - r_{x_3})} < 0$ and $\lambda_5 = -\dfrac{1}{(\mu_{x_5} - r_{x_5})} < 0$. It follows that W^* is asymptotically stable. Now consider,

$$D_Z G(W^*, 0)Z - G(W, Z) = \begin{pmatrix} M_{11} & 0 & 0 & 0 & 0 \\ M_{21} & M_{22} & 0 & 0 & 0 \\ 0 & 0 & M_{44} & 0 & 0 \\ 0 & 0 & M_{64} & M_{66} & 0 \\ M_{71} & 0 & 0 & 0 & M_{77} \end{pmatrix} \begin{pmatrix} x_1 \\ x_2 \\ x_4 \\ x_6 \\ x_7 \end{pmatrix} - \begin{pmatrix} M_{17} + M_{11}x_1 \\ M_{21}\left(1 - \dfrac{x_2}{\omega}\right)x_1 + M_{22}x_2 \\ M_{46} + M_{44}x_4 \\ M_{64}x_4 + M_{66}x_6 \\ M_{71}x_1 + M_{77}x_7 \end{pmatrix} = \begin{pmatrix} -r_{x_1} \\ \dfrac{\alpha x_1 x_2}{\omega} \\ -r_{x_4} \\ 0 \\ 0 \end{pmatrix} = \hat{0}^T$$

by (8). Hence, $\mathcal{E}_0$ is GAS.

Proof **3(b)**: For $\gamma = 0$ and $\beta = 1$, it can be shown that

$$\hat{G}(W, Z) = D_Z G(W^*, 0)Z - G(W, Z) = \left(-r_{x_1}, \frac{\alpha x_1 x_2}{\omega}, r_{x_4} - r_{x_4}x_6, 0, -N_{x_7}\mu_{x_1}\delta x_6 \right)^T = \hat{0}^T$$

by (8). Hence, $\hat{\mathcal{E}}_0$ is GAS.

Proof 3(**c**): The case $\gamma = \beta = 1$ is similar to 3(**b**). $\square$

3.3. Model Parameters

The parameter values are as given in Table 2 where the estimated parameters are derived from the simulations. We consider the chronic phase of HIV-1 infection, that is two years post infection.

Table 2
Variables and parameter values.

Variables	Initial values		Units	Reference
x_1	$x_1(0) = 5 \times 10^2$		cells mL^{-1}	[19]
x_2	$x_2(0) = 2 \times 10^2$		cells mL^{-1}	Estimated
x_3	$x_3(0) = 5 \times 10^5$		cells mL^{-1}	[1]
x_4	$x_4(0) = 10^2$		cells mL^{-1}	[4]
x_5	$x_5(0) = 5 \times 10^2$		cells mL^{-1}	Estimated
x_6	$x_6(0) = 2 \times 10^5$		virions mL^{-1}	[4]
x_7	$x_7(0) = 6.4 \times 10^4$		virions mL^{-1}	[19]

Parameters	Range	Value	Units	Reference
Death/ clearance rates				
μ_{x_1}	[0.2, 0.5]	0.33	day^{-1}	[22, 39]
μ_{x_3}	[0.001, 0.04]	0.03	day^{-1}	[18]
μ_{x_4}	$[1.1 \times 10^{-4}, 2.5 \times 10^{-4}]$	1.87×10^{-4}	day^{-1}	[28, 50]
μ_{x_5}	[0.008, 0.4]	0.3	day^{-1}	[22, 39]
μ_{x_6}	[0.1, 5]	0.1	day^{-1}	[1, 18]
μ_{x_7}	[0.35, 0.69]	0.57	day^{-1}	[12]
Source terms				
s_{x_3}	$[3 \times 10^2, 9 \times 10^5]$	3×10^3	cells mL^{-1}	[44]
s_{x_5}	$[10^3, 2 \times 10^3]$	1.1×10^3	cells mL^{-1}	Estimated
Proliferation rates				
r_{x_1}	[1, 12]	5	day^{-1}	Estimated
r_{x_3}	$[2 \times 10^{-9}, 10^{-5}]$	2×10^{-6}	day^{-1}	[18, 42]
r_{x_4}	[1, 12]	3	day^{-1}	Estimated
r_{x_5}	$[10^{-9}, 10^{-6}]$	1.2×10^{-8}	day^{-1}	Estimated
δ	$[3 \times 10^{-8}, 3 \times 10^{-4}]$	3×10^{-8}	day^{-1}	Estimated
Constants				
γ	[0,1]	variable		
β	[0,1]	variable		
Growth rates				
α	[2, 6]	2	day^{-1}	Estimated
Killing rates				
κ_1	$[1.2 \times 10^{-4}, 10^{-2}]$	9.9×10^{-3}	mL cell^{-1} day^{-1}	[22, 39]
κ_3	$[8 \times 10^{-7}, 5 \times 10^{-4}]$	3×10^{-4}	mL cell^{-1} day^{-1}	[25]
κ_4	$[10^{-5}, 2 \times 10^{-4}]$	9×10^{-5}	mL cell^{-1} day^{-1}	[42]
Maximum cell population				
ω	$[1.2 \times 10^5, 5 \times 10^6]$	1.2×10^5	cells mL^{-1}	[44]
Maximum carrying capacity				
N_{x_6}	$[10^3, 5.4 \times 10^4]$	1000	virions cell^{-1}	[20]
N_{x_7}	$[2 \times 10^2, 10^3]$	900	virions cell^{-1}	[19]

3.3.1. Model Variables and Parameters

We consider $x_1(0) = 5 \times 10^2$ cells mL^{-1} and $x_7(0) = 6.4 \times 10^4$ virions mL^{-1} as in Hadinoto *et al.* [19]. Based on Bajaria [1], we take the initial HIV-1 specific effector cell population to be $x_3(0) = 5 \times 10^5$ cells mL^{-1}, the initial infected CD4$^+$ T-cell population to be $x_4(0) = 10^2$ cells mL^{-1} and the initial HIV-1 population to be $x_6(0) = 2 \times 10^5$ virions mL^{-1} based on Boer *et al.* [4]. The estimated initial KS cell population is taken to be $x_2(0) = 2 \times 10^2$ cells mL^{-1} based on a study by Louzoun *et al.* [25] and we estimate $x_5(0) = 5 \times 10^2$ cells mL^{-1} in accordance with a study by Szomolay and Lungu.

Huynh [22] and Shapiro *et al.* [39] took the death rate of infected B-cells for the Epstein-Barr virus (EBV) infection to be $\mu_{x_1} = 0.33$ day^{-1}. HHV-8 and EBV are different viruses but due to absence of a clinical value for this parameter, we used $\mu_{x_1} = 0.33$ day^{-1} (as in [22, 39]). We assume the death rates for HIV-1 and HHV-8 specific effector cells to

be $\mu_{x_3} = 0.03$ day^{-1} as in Gumel *et al.* [18] and $\mu_{x_5} = 0.3$ day^{-1} as in [22, 39]. Based on the research by Mclean [28] and Weston [50], we took the lytic death rate of infected CD4$^+$ T-cells to be $\mu_{x_4} = 1.87 \times 10^{-4}$ day^{-1}. The estimated clearance rate of HIV-1 virus, μ_{x_6}, is taken to be in the range $0.1 - 5$ day^{-1} based on a study by Bajaria and Gumel [1, 18]. Due to the absence of estimates for the virus half life of HHV-8, we will use the value in a study by Foglieni *et al.* [12] which is $\mu_{x_7} = 0.57$ day^{-1}.

Based on a study by Szomolay and Lungu [44], we take the range $s_{x_3} = 3 \times 10^2 - 9 \times 10^5$ cells mL^{-1} and we estimate the value of s_{x_5} to be 1.1×10^3 cells mL^{-1}.

The proliferation rate of HIV-1 specific effector cells are taken from studies by Gumel [18] and Stilianakis [42]. In these studies r_{x_3} is assumed to be 2×10^{-6} day^{-1}. Due to absence of HHV-8 proliferation rates, we have estimated $r_{x_5} = 1.2 \times 10^{-8}$ day^{-1}. We estimate r_{x_1} and r_{x_4} to be in the range $2 - 12$ day^{-1}, the range for δ is estimated to be in the region 3×10^{-8} to 3×10^{-4} day^{-1}.

We estimate the cancer growth rate α to be 2 day^{-1} and we have used the killing rate of infected B-cells $\kappa_1 = 9.9 \times 10^{-3}$ mL cell^{-1} day^{-1}. Based on Louzoun [25], the killing rate of KS cells is taken to be $\kappa_3 = 3 \times 10^{-4}$ mL cell^{-1} day^{-1}. The killing rate of infected CD4$^+$ T-cells is $\kappa_4 = 9 \times 10^{-5}$ mL cell^{-1} day^{-1} as in Stilianakis [42]. Following Szomolay and Lungu [44], we take $\omega = 1.2 \times 10^5$ cells. We take the total burst size of infected CD4$^+$ T-cells, N_{x_6} to be in the range $10^3 - 5 \times 10^4$ virions day^{-1} as in Boer [4]. The range for N_{x_7} is taken to be $2 \times 10^2 - 10^3$ virions cell^{-1} based on Hadinoto [19].

4. Sensitivity Analysis for the Weak Viral Source Model

In determining how best to treat KS infection, it is necessary to know the relative importance of the different factors responsible for its transmission. In this section we analyse the sensitivity of $\mathcal{R}_{0x_6}$ and $\mathcal{R}_{0x_7}$ to the parameters in the model. If the reproduction number is very sensitive to a particular parameter, then a perturbation of the conditions that connect the dynamics to such a parameter may prove useful in identifying policies or intervention strategies that reduce KS prevalence.

We explore the parameter space by performing an uncertainty analysis using Latin Hypercube Sampling (LHS) method as described by Blower and Gomero [3, 16]. Coeffcients (PRCC) are used to evaluate the contribution of vital parameters on the model dynamics, most specifically to establish the parameters that have significant influence on the HIV-related KS. MATLAB software was used for the PRCC analysis with a sampling size, $n = 1000$.
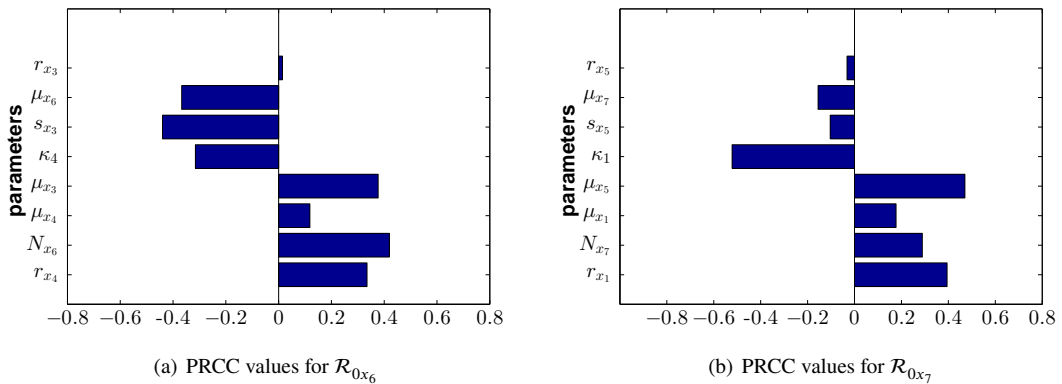

(a) PRCC values for $\mathcal{R}_{0x_6}$

(b) PRCC values for $\mathcal{R}_{0x_7}$

Figure 2: Sensitivity of $\mathcal{R}_{0x_6}$ and $\mathcal{R}_{0x_7}$ to some of the parameters.

PRCC is the tool we use to evaluate the impact of changes of each parameter on $\mathcal{R}_{0x_6}$ and $\mathcal{R}_{0x_7}$. It is informative on what parameters to target in order to achieve specific goals for example how to effectively reduce VL and KS. Figure 2(a) shows the PRCC results which illustrate the dependence of $\mathcal{R}_{0x_6}$ on each parameter. The positive signs of their PRCCs indicate that if the parameters are increased, the value of $\mathcal{R}_{0x_6}$ increases and vice versa. The following parameters have a statistically significant PRCC value and a negative influence on $\mathcal{R}_{0x_6}$: κ_4, s_{x_3} and μ_{x_6} while the the

opposite is true for r_{x_4}, N_{x_6}, μ_{x_4}, r_{x_3} and μ_{x_3}. Predominantly, s_{x_3} has the greatest influence on $\mathcal{R}_{0x_6}$. Figure 2(b) shows the PRCC results which illustrate the dependence of $\mathcal{R}_{0x_7}$ on each parameter. The following HHV-8 associated parameters have a statistically significant PRCC value and have the potential to positively influence infection: r_{x_1}, N_{x_7}, μ_{x_1} and μ_{x_5} and the opposite is true for κ_1, s_{x_5}, r_{x_5} and μ_{x_7}. The most significant control parameter for $\mathcal{R}_{0x_7}$ is κ_1.

The significance of the PRCC for each parameter is determined by calculating a p-value for each using the methods described by Marino *et al.* [27]. The PRCC values with a p-value less than 0.01 are considered statistically significant. From Tables 3 and 5, it can be seen that r_{x_3} and r_{x_5} are not statistically significant.

In order to test for independence between the parameters which affect the reproduction numbers, we apply the Fisher transformation to the PRCC as described by Fieller *et al.*[11]. We use R software is to test for independence. We corrected the resulting p-values for false discovery using the false discovery rate (FDR) method of Benjamini and Hochberg [2]. Using the parameters whose PRCC values were found to be significant, we performed pairwise comparisons with Fisher transformed values [11], hence produces the results given in Table 4. A red TRUE indicates independence between two parameters a black FALSE indicates the opposite. The independence test indicates that s_{x_3} may be influenced by μ_{x_6} as illustrated in Table 4.

Table 3
PRCC for $\mathcal{R}_{0x_6}$ and p-values resulting from the sensitivity analysis.

Variable	PRCC	$p-$value
r_{x_4}	0.3350	0.000
N_{x_6}	0.4195	0.000
μ_{x_4}	0.1183	1.842×10^{-4}
μ_{x_3}	0.3771	0.000
κ_4	-0.31534	0.000
s_{x_3}	-0.4399	0.000
μ_{x_6}	-0.3673	0.000
r_{x_3}	0.0145	6.482×10^{-1}

Table 4
Pairwise comparisons for $\mathcal{R}_{0x_6}$ parameters. .

	N_{x_6}	μ_{x_4}	μ_{x_3}	κ_4	s_{x_3}	μ_{x_6}
r_{x_4}	TRUE	TRUE	FALSE	TRUE	TRUE	TRUE
N_{x_6}		TRUE	FALSE	TRUE	TRUE	TRUE
μ_{x_4}			TRUE	TRUE	TRUE	TRUE
μ_{x_3}				TRUE	TRUE	TRUE
κ_4					TRUE	FALSE
s_{x_3}						FALSE

Table 5
PRCC for $\mathcal{R}_{0x_7}$ and p-values resulting from the sensitivity analysis.

Variable	PRCC	p $-$ value
r_{x_1}	0.3944	0.000
N_{x_7}	0.2890	0.000
μ_{x_1}	0.1771	1.784×10^{-8}
μ_{x_5}	0.4705	0.000
κ_1	-0.5217	0.000
s_{x_5}	-0.1035	1.082×10^{-3}
μ_{x_7}	-0.1552	8.521×10^{-7}
r_{x_5}	-0.0320	3.138×10^{-1}

Table 6
Pairwise comparisons for $\mathcal{R}_{0x_7}$ parameters.

	N_{x_7}	μ_{x_1}	μ_{x_5}	κ_1	s_{x_5}	μ_{x_7}
r_{x_1}	TRUE	TRUE	TRUE	TRUE	TRUE	TRUE
N_{x_7}		TRUE	TRUE	TRUE	TRUE	TRUE
μ_{x_1}			TRUE	TRUE	TRUE	TRUE
μ_{x_5}				TRUE	TRUE	TRUE
κ_1					TRUE	TRUE
s_{x_5}						FALSE

5. Numerical Simulations for the Weak Viral Source Model without Optimal Control

In order to examine the progression of the infection, we consider the following scenarios: (i) $\gamma = \beta = 0$, (ii) $\gamma = 0$ and $\beta = 1$ and (iii) $\gamma = \beta = 1$. Figure 3 shows the prognosis of the infection for $\gamma = \beta = 0$. This case demonstrates a scenario when both infected CD4$^+$ T-cells and B-cells divide at a constant rate (Cho *et al.* [9]). Figure 3(a) shows that after reaching a peak during the primary stage, the HIV-1 VL, x_6, decays below a detectable level of 100 virions per microliter of blood [32]. A similar pattern is observed for HHV-8, x_7. In response, both HIV-1 and HHV-8 specific effector cells, x_3 and x_5, respectively increase to a peak and remain constant throughout the chronic stage (3(b)). Figure 3(a) shows that the infected B- and CD4$^+$ T-cells, x_1 and x_4, respectively decrease due to lysing by the increasing populations of respective effector cells. Figure 3(b) shows that the population of KS cells declines. KS cannot develop into a clinical condition for $\gamma = \beta = 0$. The WHO guidelines are not available for us to conclude whether this steady state, below 100 copies/mL, is detectable or undetectable for KS.

Figure 4 illustrates the case when the infected B-cells are dividing slowly and the infected CD4$^+$ T-cells are dividing rapidly. We demonstate the case for $\gamma = 0$ and $\beta = 1$. We can see that HIV-1 VL is high but HHV-8 VL is low. The infected CD4$^+$ T-cell population is also high but the infected B-cell population is low. The prognosis for the KS is low suggesting that cell division for infected B-cells plays a very important role. The high population of HHV-8 specific effector cells, x_5, suggests a high rate of lysing of KS cells.

Figure 5 describes disease progression for $\gamma = \beta = 1$. This case represents a scenario when both infected CD4$^+$ T-cells and B-cells divide rapidly. Figure 5(a) shows prolonged and severe viremia for both HIV-1 and HHV-8. The VLs remain detectable throughout the chronic stage. Figure 5(a) shows a high population level for infected CD4$^+$ T-cells. The HIV-1 and HHV-8 specific effector cell populations remain high throughout and consequently the KS cells population remains high improving the chances of KS development. (Figure 5(b)). With a low cancer burden representing only 0.001% of maximum carrying capacity of KS cells, the HHV-8 load will reach equilibrium that is either below the level of detection ($\gamma = 0$ and $\beta \geq 0$), or above ($\gamma = \beta = 1$). In the latter case, over 3000-fold increase in HHV-8 load is obtained compared to the level off detection and the KS load increases to 2.7% of the maximum carrying capacity (Figure 13 in Appendix A.4).
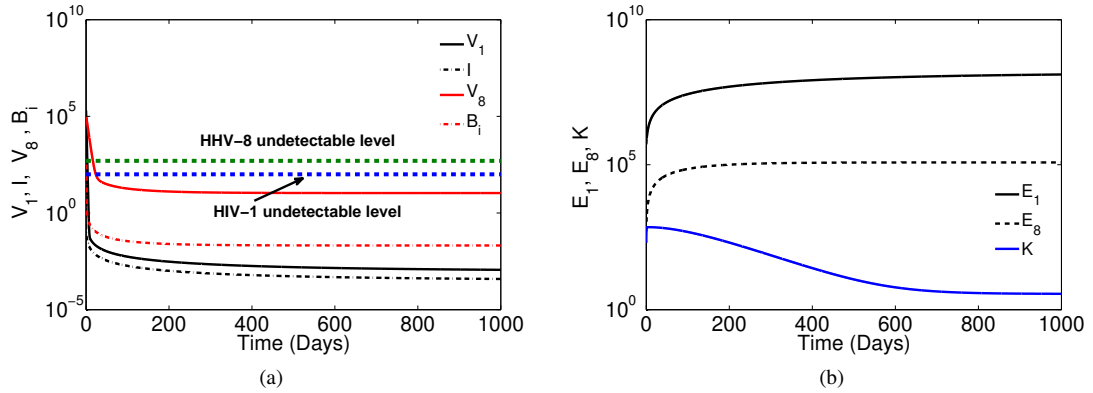
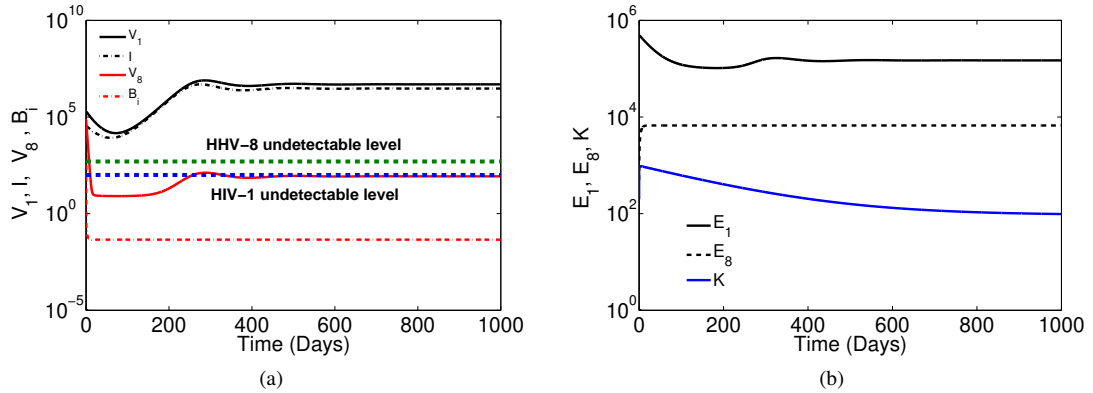**Figure 3:** Population dynamics with $\gamma = \beta = 0$.

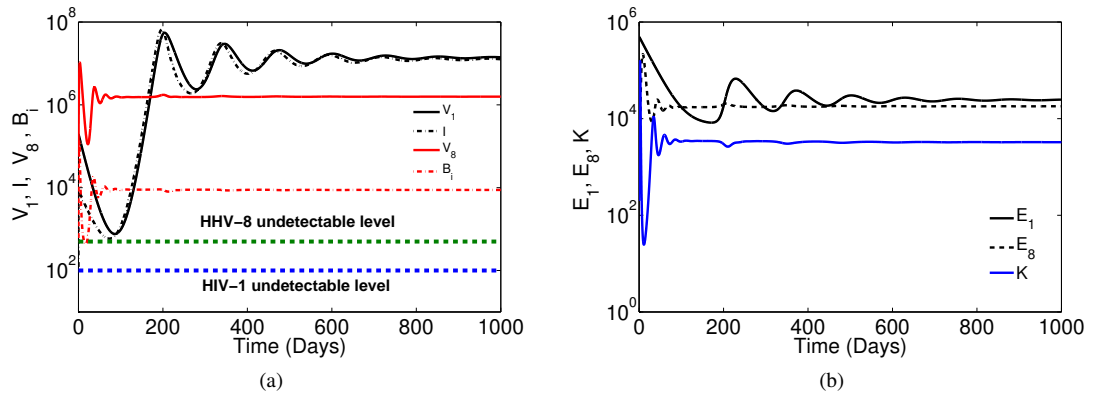**Figure 4:** Population dynamics with $\gamma = 0$ and $\beta = 1$.

Figure 5: Population dynamics with $\gamma = \beta = 1$.

6. Strong Viral Source Model with $H_1(x_6, \beta) = x_6^\beta + x_6$ and $H_8(x_7, \gamma) = x_7^\gamma + x_7$

In this section, we consider the model with strong viral source that may be caused by many factors such as non-adherence to treatment. Adherence to HAART helps maintain low to undetectacle VL. However, non-adherence leads to higher number of infected cells and consequently to an increase in the VL as indicated by Turner and WHO [45, 33]. The new system (1)*–(7)* will be essentially the same as (1) – (7) except that $H_1(x_6, \beta) = x_6^\beta + x_6$ and $H_8(x_7, \gamma) = x_7^\gamma + x_7$. We note that (1)*–(7)* can be rewritten as $\dot{x} = \mathbf{A}x^\gamma + \mathbf{C}x$, where matrix $\mathbf{A}$ is defined in (9) and matrix $\mathbf{C}$ is defined in (11). We consider the cases (i)-(iii) as in Section 2.

6.1. Stability Analysis Case (i)

Consider the case $\gamma = \beta = 0$. The system (1)*–(7)* reduces to $\dot{x} = \mathbf{M}x$, where the matrix $\mathbf{M}$ is given in A.1. The coefficients of the characteristic polynomial $P(\lambda) = \lambda^4 + \sum_{j=1}^{4} a_j \lambda^{4-j}$, associated with $\mathbf{M}$, are given by a_1, a_2, a_3, and a_4 (shown in A.2). In this case the term $(1 - \mathcal{R}_{0x_i})$ is replaced by $(1 - \mathcal{R}_{0x_i}^\star)$ with $\mathcal{R}_{0x_i}^\star = \text{Max}[\mathcal{R}_{0x_6}^\star, \mathcal{R}_{0x_7}^\star]$, where $\mathcal{R}_{0x_6}^\star = \mathcal{R}_{0x_6}$ and $\mathcal{R}_{0x_7}^\star = (1 + \delta)\mathcal{R}_{0x_7}$.

Theorem 4. *For $\gamma = \beta = 0$ the VFE, $\mathcal{E}_0$, is stable if $\mathcal{R}_{0x_i}^\star < 1$, otherwise it is unstable.*

Remark 1. *In this case the reproduction number is not zero as in Section 3.*

6.2. Stability Analysis Case (ii)

When $\gamma = 0$ and $\beta = 1$, the system (1)*–(7)* becomes $\dot{x} = \mathbf{N}x$, where

$$\mathbf{N} = \begin{pmatrix} M_{11} & 0 & 0 & 0 & 0 & 0 & M_{17} \\ M_{21} & M_{22} & 0 & 0 & 0 & 0 & 0 \\ 0 & 0 & M_{33} & 0 & 0 & 2M_{36} & 0 \\ 0 & 0 & 0 & M_{44} & 0 & 2M_{46} & 0 \\ 0 & 0 & 0 & 0 & M_{55} & 0 & M_{57} \\ 0 & 0 & 0 & M_{64} & 0 & M_{66} & 0 \\ \frac{M_{71}}{1+\delta} & 0 & 0 & 0 & 0 & 0 & M_{77} \end{pmatrix}$$

The term $(1 - \mathcal{R}_{0x_i})$ in the coefficients of the characteristic polynomial given in A.2, is replaced by $(1 - \bar{\mathcal{R}}_{0x_i})$. We have $\bar{\mathcal{R}}_{0x_i} = \text{Max}[\bar{\mathcal{R}}_{0x_6}, \bar{\mathcal{R}}_{0x_7}]$ where $\bar{\mathcal{R}}_{0x_6} = 2\mathcal{R}_{0x_6}$ and $\bar{\mathcal{R}}_{0x_7} = \mathcal{R}_{0x_7}$.

Theorem 5. *For $\gamma = 0$ and $\beta = 1$ the VFE, $\mathcal{E}_0$, is stable if $\bar{\mathcal{R}}_{0x_i} < 1$, otherwise it is unstable.*

6.2.1. Stability Analysis Case (iii)

When $\gamma = \beta = 1$, the system (1)*–(7)* can be written as $\dot{x} = \mathbf{D}x$, where $\mathbf{D} = \mathbf{A} + \mathbf{C}$ and matrix $\mathbf{A}$ is defined in (9) and matrix $\mathbf{C}$ is defined in (11). The term $(1 - \mathcal{R}_{0x_i})$ in the coefficients of the characteristic polynomial given in A.2, is replaced by $(1 - \bar{\mathcal{R}}_{0x_i})$, where $\hat{\mathcal{R}}_{0x_i} = 2\mathcal{R}_{0x_i}$.

Remark 2. *The case $\gamma = \beta = 1$ leads to doubling of the reproduction number. Non-adherence to treatment results in increased reproduction number and can complicate treatment. Nachega et al. [29] has pointed out that adherence to HAART supresses viral replication and leads to slow cell division.*

Remark 3. *Generally some patients are immunologically susceptible to high VL production. Such patients should be identified through screening (regular checkups) and made to start their treatment early.*

6.3. Numerical Simulations

Figure 6 depicts the population dynamics of virions and cell population when the VL is high for the case when $\gamma = \beta = 0$. HIV-1 and HHV-8 VLs remain high throughout the chronic stage, consequently, high levels of infected CD4$^+$ T-cells and B-cells are observed in Figure 6(a). This results in high levels of KS as shown in Figure 6(b). The immune response remains high due to the high levels of infected CD4$^+$ T-cells and B-cells (Figure 6(b)). The pattern observed here is similar to that observed in Figure 5 for the low VL model when $\gamma = \beta = 1$.
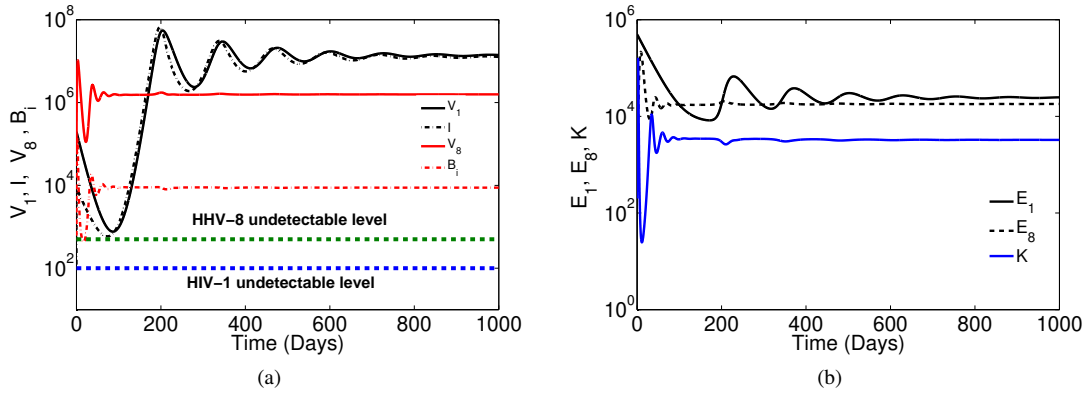
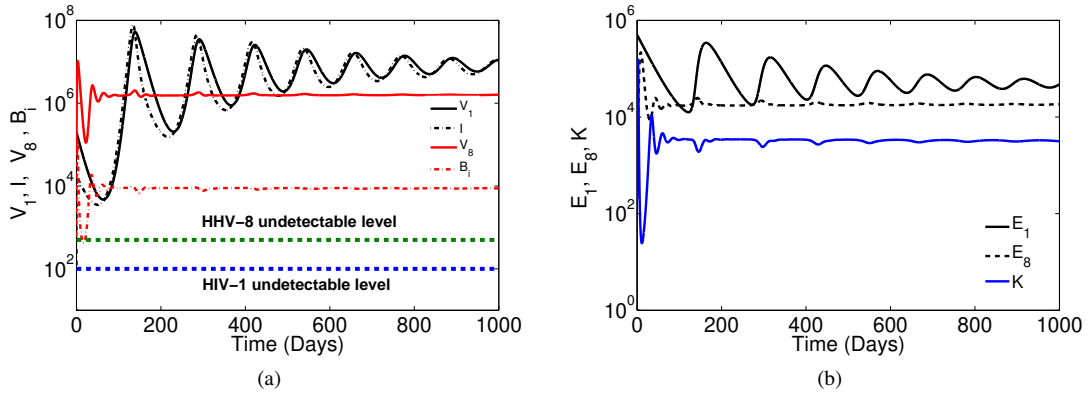**Figure 6:** Population dynamics with $\gamma = \beta = 0$.

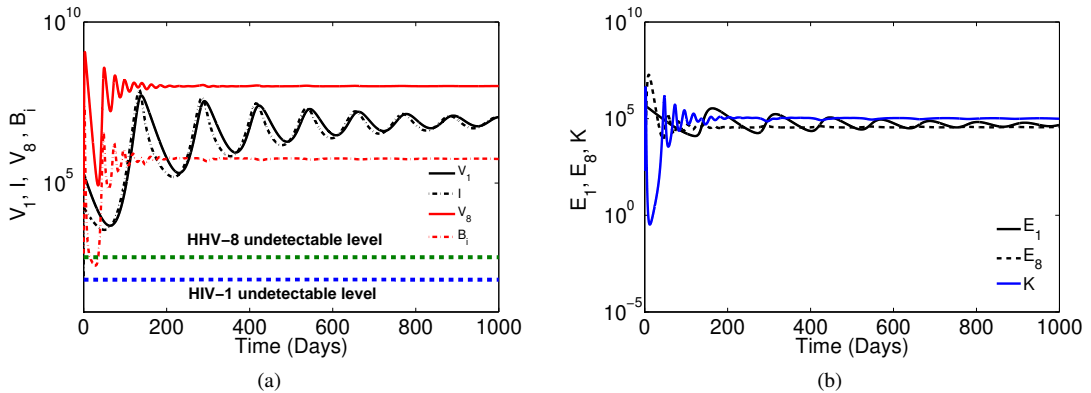**Figure 7:** Population dynamics with $\gamma = 0$ and $\beta = 1$.

Figure 8: Population dynamics with $\gamma = \beta = 1$.

Figure 7 illustrates the case when $\gamma = 0$ and $\beta = 1$. HIV-1 and HHV-8 VLs remain above detectable levels throughout the infection as seen in Figure 7(a). Due to high levels of HIV-1 and HHV-8 VLs, the infected CD4$^+$ T-cell and B-cell populations remain high as shown in Figure 7(a). Consequently (as seen in Figure 7(b)), the KS population remains high due to high levels of HHV-8. In response, the HIV-1 and HHV-8 specific effector cell populations remain high as illustrated in Figure 7(b). The cell levels in Figure 7 are significantly higher than those in Figure 6.

Figure 8 shows the case when $\gamma = \beta = 1$, that is when both infected CD4$^+$ T-cells and infected B-cells divide faster. A similar behavior to that in Figure 7 is observed. From Figures 7 and 8, we conclude that the higher the proliferation of HHV-8 due to enhancement by HIV-1 has more impact on the development of KS than the increase in the infected B-cell population.

Although the equilibria for the strong viral source model when $\gamma = 0$ and $\beta \geq 0$ do not change substantially, there is a profound impact on KS and HHV-8 burden when $\gamma = \beta = 1$. In the latter case the KS load increases to over 80% of the maximum carrying capacity of KS cells and the HHV-8 load over 200000-fold above the level of HHV-8 detection, surpassing even the HIV-1 load (Figure 14 in Appendix A.4).

7. Optimal Control for the Weak Viral Source Model

We will apply optimal control methods to find the optimal dosage scheme for cART comprising of HAART and KS therapy that minimizes the infected CD4$^+$ T-cell count, KS tumor burden and drug toxicity. HAART involves the usage of multiple forms of antiretroviral agents, typically RTIs and PIs, whose efficacy is denoted by ζ_r and ζ_p, respectively. The RTIs are inhibiting the HIV virions from successfully infecting the cell and the PIs prevent the already infected cells from producing mature infectious virions as highlighted by Perelson [35]. The KS therapy can involve chemotherapy or interferon therapy and its efficacy is expressed by η_c.

We formulate an optimal control problem (OCP) by considering cART to minimise the number of infected CD4$^+$ T-cells, KS cells and the cost of treatment (e.g. drug toxicity, cytokine storm) over a given time interval $[0, t_f]$. Our goal is to determine the efficacy functions $0 \leq \zeta_r, \zeta_p, \eta_c \leq 1$ that minimize the objective functional given by

$$J(\zeta_r, \zeta_p, \eta_c) = \int_0^{t_f} (A_1 x_4 + A_2 x_2 + A_3 \zeta_r^2 + A_4 \zeta_p^2 + A_5 \eta_c^2) \, dt, \tag{13}$$

where x_2, x_4 are solutions of the system (1)–(7) with $H_1(x_6, \beta) = x_6^\beta$ and $H_8(x_7, \gamma) = x_7^\gamma$. The efficacy functions ζ_r, ζ_p, η_c are bounded and Lebesgue integrable as was indicated by Lenhart and Workman [41]. The case $\zeta_r = \zeta_p = \eta_c = 1$ represents total efficacy for the RTIs, PIs and KS therapy, respectively, and $\zeta_r = \zeta_p = \eta_c = 0$ represents no treatment. As studied in Holash et al. [21], the delivery time frame for anti-angiogenesis treatment is two to three weeks. This research defines the treatment time as 30 days in order to compare with the clinical studies already done, and allows for an easier transition from current practice to the proposed dosing scheme.

The coefficients A_i where $i = 1, 2, 3, 4, 5$ are positive weights to balance the factors and the term $A_1 x_4$ and $A_2 x_2$ are cost of infection while $A_3 \zeta_r^2$, $A_4 \zeta_p^2$ and $A_5 \eta_c^2$ are the cost associated with controls. The quadratic control in the treatment terms has the advantage of keeping the infection in check both when it is small or large in size, see for example, Kirschner et al. [24] and Pillis et al. [37]. Furthermore, the quadratic control allows for optimal treatment to minimize the toxicity while permitting the system to maintain a low KS tumor burden. It is worth noting that ζ_r^2, ζ_p^2 and η_c^2 parameters in the integrand of Equation (13) denote what is referred to as a continuous optimal control. Continuous optimal control ensures that the drugs are being applied continuously over the entire treatment period and ensure that there is no biological drug clearance from the patient's system.

We seek efficacy functions ζ_r, ζ_p and η_c such that

$$J(\zeta_r^*, \zeta_p^*, \eta_c^*) = min\{J(\zeta_r, \zeta_p, \eta_c) : \zeta_r, \zeta_p, \eta_c \in U\},$$

where U is the control set defined by

$$U = \{(\zeta_r, \zeta_p, \eta_c) : \zeta_r, \zeta_p, \eta_c \text{ is Lebesgue measurable}, 0 \leq \zeta_r, \zeta_p, \eta_c \leq 1, t \in [0, t_f]\}. \tag{14}$$

7.1. Existence and Uniqueness of Optimal Control

Theorem 6. *There exists an optimal control $u *= (\zeta_r^*, \zeta_p^*, \eta_c^*)$ such that $min_{\zeta_r, \zeta_p, \eta_c \in U} J(\zeta_r, \zeta_p, \eta_c) = J(\zeta_r^*, \zeta_p^*, \eta_c^*)$ subject to the OCP (1)–(7) with (13) and non-negative initial conditions.*

Proof. To prove the existence of an optimal control we note that the control and state variables are nonnegative values. In this minimizing problem, the necessary convexity of the objective functional in ζ_r, ζ_p and η_c is satisfied. The set of all the control variables $(\zeta_r, \zeta_p, \eta_c) \in U$ are also convex and closed by definition. The optimalitty system is bounded which determines the compactness needed for the existence of the optimal control. In addition, the integrand in the functional (13), $A_1 x_4 + A_2 x_2 + A_3 \zeta_r^2 + A_4 \zeta_p^2 + A_5 \eta_c^2$ is convex on the control set U. There exist a constant $\rho > 1$ and positive numbers ϵ_1 and ϵ_2 such that $J(\zeta_r, \zeta_p, \eta_c) \geq \epsilon_2 + \epsilon_1 (|\zeta_r|^2 + |\zeta_p|^2 + |\eta_c|^2)^{\rho/2}$. This implies that

$$A_1 x_4 + A_2 x_2 + A_3 \zeta_r^2 + A_4 \zeta_p^2 + A_5 \eta_c^2 \geq \epsilon_2 + \epsilon_1 (|\zeta_r|^2 + |\zeta_p|^2 + |\eta_c|^2)$$

where ϵ_2 depends on the upper bound on x_2 and x_4 and $\epsilon_1 > 0$ since $A_3 > 0$, $A_4 > 0$ and $A_5 > 0$. The uniqueness of the optimal control follows from the uniqueness of the optimality system which is guaranteed by the finite time interval. □

7.2. Necessary Conditions for the Existence of Optimal Control

In order to find the optimal solutions, we first trace the Lagrangian and Hamiltonian for the OCP (1)–(7) with (13). The Lagrangian of the OCP is given by:

$$L(x_1, x_2, x_3, x_4, x_5, x_6, x_7, \zeta_r, \zeta_p, \eta_c) = A_1 x_4 + A_2 x_2 + A_3 \zeta_r^2 + A_4 \zeta_p^2 + A_5 \eta_c^2 \tag{15}$$

Pontryagin's Maximum Principle (see Lenhart and Workman [41]) is applied to determine the conditions for effective control. This principle converts the system (1)–(7) with (13)-(14) into a problem of minimising a Hamiltonian pointwisely with respect to ζ_r, ζ_p and η_c. We define the Hamiltonian, H, for the OCP:

$$H = L(x_1, x_2, x_3, x_4, x_5, x_6, x_7, \zeta_r, \zeta_p, \eta_c) + \sum_{i=1}^{7} \lambda_i f_i$$

where L is the Lagrangian function (15), λ_i, $i = 1, 2...7$ are the adjoints variables (co-state variables) for the states $x_1, x_2, x_3, x_4, x_5, x_6, x_7$. and f_i is the right hand side of the differential equation of i-th state variable. Our aim is to seek an optimal control pair (u^*, X^*) where $u* = (\zeta_r^*, \zeta_p^*, \eta_c^*)$ and $X^* = (x_1^*, x_2^*, x_3^*, x_4^*, x_5^*, x_6^*, x_7^*)$, that minimizes the Hamiltonian of the system given by:

$$H = A_1 x_4 + A_2 x_2 + A_3 \zeta_r^2 + A_4 \zeta_p^2 + A_5 \eta_c^2 + \lambda_1 [r_{x_1} x_7^\gamma - \mu_{x_1} x_1 - \kappa_1 x_1 x_5] + \lambda_2 [(1 - \eta_c)\alpha x_1 \left(1 - \frac{x_2}{\omega}\right) - \kappa_3 x_2 x_5]$$

$$+ \lambda_3 [s_{x_3} + r_{x_3} x_3 x_6^\beta - \mu_{x_3} x_3] + \lambda_4 [(1 - \zeta_r) r_{x_4} x_6^\beta - \kappa_4 x_3 x_4 - \mu_{x_4} x_4] + \lambda_5 [s_{x_5} + r_{x_5} x_5 x_7^\gamma - \mu_{x_5} x_5]$$

$$+ \lambda_6 [(1 - \zeta_p) N_{x_6} \mu_{x_4} x_4 - \mu_{x_6} x_6] + \lambda_7 [N_{x_7} \mu_{x_1} x_1 (1 + \delta x_6^\beta) - \mu_{x_7} x_7]$$

Pontryagin's Maximum Principle gives the necessary conditions for the existence of an optimal solution. The results of applying Pontryagin's Maximum Principle lead to the following theorem:

Theorem 7. *(Optimal Control for the Treatment Model). There exists an optimal control ζ_r^*, ζ_p^*, η_c^* and the corresponding solutions $(x_1^*, x_2^*, x_3^*, x_4^*, x_5^*, x_6^*, x_7^*)$ that minimizes $J(\zeta_r, \zeta_p, \eta_c)$ over U. Furthermore, there exists adjoint variables λ_i, $i = 1, 2...7$ which satisfy*

$$\dot{\lambda}_1 = \lambda_1 (\mu_{x_1} + \kappa_1 x_5) - \lambda_2 \alpha (1 - \eta_c) \left(1 - \frac{x_2}{\omega}\right) - \lambda_7 N_{x_7} \mu_{x_1} (1 + \delta x_6^\beta),$$

$$\dot{\lambda}_2 = \lambda_2 [(1 - \eta_c)\alpha \frac{x_1}{\omega} + \kappa_3 x_5] - A_2,$$

$$\dot{\lambda}_3 = \lambda_4 \kappa_4 x_4 - \lambda_3 (r_{x_3} x_6^\beta - \mu_{x_3}),$$

$$\dot{\lambda}_4 = \lambda_4 (\kappa_4 x_3 + \mu_{x_4}) - \lambda_6 (1 - \zeta_p) N_{x_6} \mu_{x_4} - A_1,$$

$$\dot{\lambda}_5 = \lambda_1 \kappa_1 x_1 + \lambda_2 \kappa_3 x_2 - \lambda_5 (r_{x_5} x_7^\gamma - \mu_{x_5}),$$

$$\dot{\lambda}_6 = \lambda_6 \mu_{x_6} - \lambda_3 r_{x_3} \beta x_3 x_6^{\beta-1} - \lambda_4 (1 - \zeta_r) r_{x_4} \beta x_6^{\beta-1} - \lambda_7 N_{x_7} \mu_{x_1} \delta \beta x_1 x_6^{\beta-1},$$

$$\dot{\lambda}_7 = \lambda_7 \mu_{x_7} - \lambda_1 r_{x_1} \gamma x_7^{\gamma-1} - \lambda_5 r_{x_5} \gamma x_5 x_7^{\gamma-1}$$

with transversality conditions $\lambda_i(t_f) = 0$ for $i = 1, 2, ...7$. The optimal control is given by

$$\zeta_r^* = max\left\{ 0, min\left(\frac{\lambda_4 r_{x_4} x_6^{\beta*}}{2A_3}, 1 \right) \right\}, \quad \zeta_p^* = max\left\{ 0, min\left(\frac{\lambda_6 N_{x_6} \mu_{x_4} x_4^*}{2A_4}, 1 \right) \right\} \tag{16}$$

$$\eta_c^* = max\left\{ 0, min\left(\frac{1}{2A_5}\left(\lambda_2 \alpha x_1^*\left(1 - \frac{x_2^*}{\omega} \right) \right), 1 \right) \right\} \tag{17}$$

Proof. Due to the convexity of the integrand of J in equation (13), a priori boundedness of the state solutions and the Lipschitz property of the state system with respect to the state variables, the adjoint equations and transversality conditions can be obtained by using Pontryagin's Maximum Principle such that $\dot{\lambda}_i = -\dfrac{\partial H}{\partial x_i}$, with transversality conditions $\lambda_i(t_f) = 0$ for $i = 1, 2, ...7$. The characterisation of the optimal control obtained by solving the optimality condition $\dfrac{\partial H}{\partial \zeta_r} = \dfrac{\partial H}{\partial \zeta_p} = \dfrac{\partial H}{\partial \eta_c} = 0$ gives the following characterisations of the controls:

$$\frac{\partial H}{\partial \zeta_r} = 2A_3 \zeta_r - \lambda_4 r_{x_4} x_6^{\beta} = 0, \quad \frac{\partial H}{\partial \zeta_p} = 2A_4 \zeta_p - \lambda_6 N_{x_6} \mu_{x_4} x_4 = 0 \quad \frac{\partial H}{\partial \eta_c} = 2A_5 \eta_c - \lambda_2 \alpha x_1\left(1 - \frac{x_2}{\omega} \right) = 0 \tag{18}$$

Solving (18) gives $\zeta_r^* = \dfrac{\lambda_4 r_{x_4} x_6^{\beta*}}{2A_3}, \quad \zeta_p^* = \dfrac{\lambda_6 N_{x_6} \mu_{x_4} x_4^*}{2A_4}$ and $\eta_c^* = \dfrac{1}{2A_5}\left(\lambda_2 \alpha x_1^*\left(1 - \dfrac{x_2^*}{\omega} \right) \right)$.

The standard control arguments on the controls are such that

$$\zeta_r^* = \begin{cases} 0 & \text{if } m_1^* \leq 0 \\ m_1^* & 0 < m_1^* < 1 \\ 1 & m_1^* \geq 1 \end{cases} \quad \text{where } m_1^* = \frac{\lambda_4 r_{x_4} x_6^{\beta*}}{2A_3} \tag{19}$$

$$\zeta_r^* = \begin{cases} 0 & \text{if } m_2^* \leq 0 \\ m_2^* & 0 < m_2^* < 1 \\ 1 & m_2^* \geq 1 \end{cases} \quad \text{where } m_2^* = \frac{\lambda_6 N_{x_6} \mu_{x_4} x_4^*}{2A_4} \tag{20}$$

$$\zeta_r^* = \begin{cases} 0 & \text{if } m_3^* \leq 0 \\ m_3^* & 0 < m_3^* < 1 \\ 1 & m_3^* \geq 1 \end{cases} \quad \text{where } m_3^* = \frac{1}{2A_5}\left(\lambda_2 \alpha x_1^*\left(1 - \frac{x_2^*}{\omega} \right) \right) \tag{21}$$

Equations (19), (20) and (21) can be written in compact form as in Equations (16)-(17). $\square$

7.3. Optimal Control Simulations

Here we show the numerical results of the OCP and we will assume that $\gamma = \beta = 1$ since the simulations remain largely unaffected by the other cases. The algorithm for simulating the system using the forward-backward sweep method is adopted from Lenhart and Workman [41]. The state system with an initial guess is solved forward in time and then the adjoint system is solved backward in time. The controls are updated at the end of each iteration using the formula for optimal controls. The iterations continue until convergence is achieved.

We take $t_f = 30$ days which represents the time in which treatment is stopped. The values of the weight function are taken as $A_1 = 10$, $A_2 = 0.01$, $A_3 = 200$, $A_4 = 100$ and $A_5 = 1000$. It should be pointed out that the weights used in the simulations are are not clinically determined but are used to illustrate the control strategies proposed for this study. The costs correspond to the case of very cheap to very expensive control strategies. The higher the value,

the more expensive the treatment. The initial variables and parameter values are taken from Table 2. The initial values are chosen such that they reflect a patient during chronic infection since the WHO recommendations stipulate that all people living with the HIV be put on HAART irrespective of their CD4$^+$ counts [32]. The reproduction number in the absence of treatment is $R_{0x_i} = 5.18$ which was obtained from using the parameter values in Table 2.

The results of the system (1)–(7) with and without controls are depicted in Figures (9) – (12). Figure 9(a) shows the HIV-1 virus population level with and without controls. We can see that the VL when the treatment is not optimal can result in very high levels. When optimal treatment is administered the VL remains low. As demonstrated by Figure 9(b), the HHV-8 population starts to decline slowly after day 3.
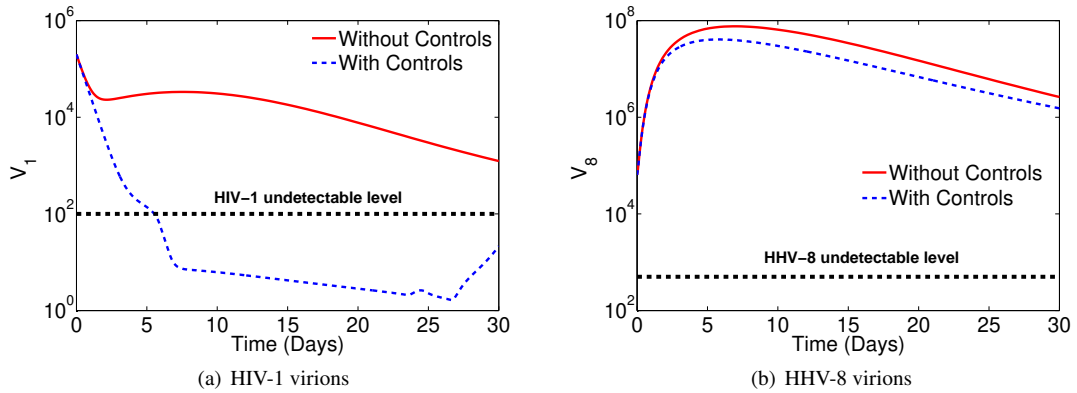

(a) HIV-1 virions

(b) HHV-8 virions

Figure 9: Virions with and without controls.

We see from Figure 10(a) that when there is no control the infected CD4$^+$ T-cell population rises and settles at some steady state level. With optimal treatment the infected CD4$^+$ T-cell population declines and remains significantly lower than the population without controls. The infected B-cell population on the other hand starts to decline slowly after day 2 when treatment is optimal (Figure 10(b)).
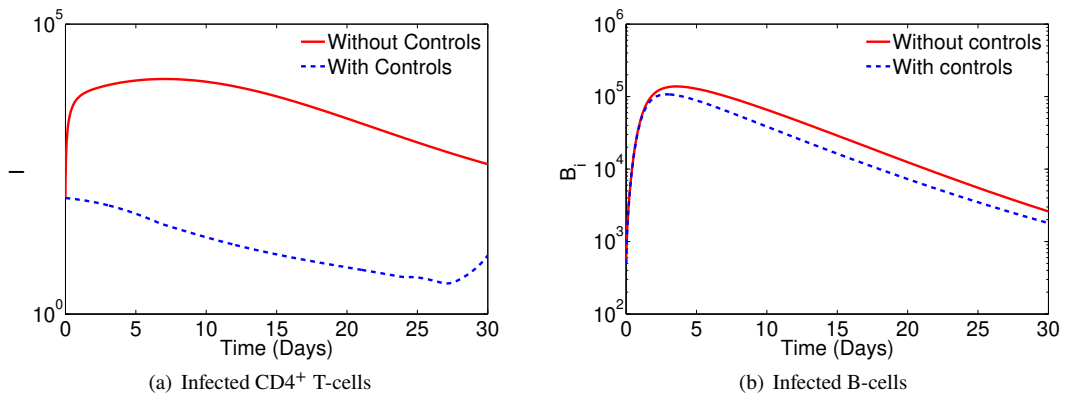

(a) Infected CD4$^+$ T-cells

(b) Infected B-cells

Figure 10: Infected cells with and without controls.

Figure (11) shows that when treatment is optimal, the HIV-1 and HHV-8 specific effector cells are not affected by treatment as expected.

Figure (12) demonstrates how the optimal treatment affects the KS development. Without treatment the KS cell population grows very fast, but when there is optimal treatment the KS cell population remains constant for most of the treatment period (Figure 12(a)). Figure 12(b) illustrates the control profiles where controls ζ_r and η_c are at upper

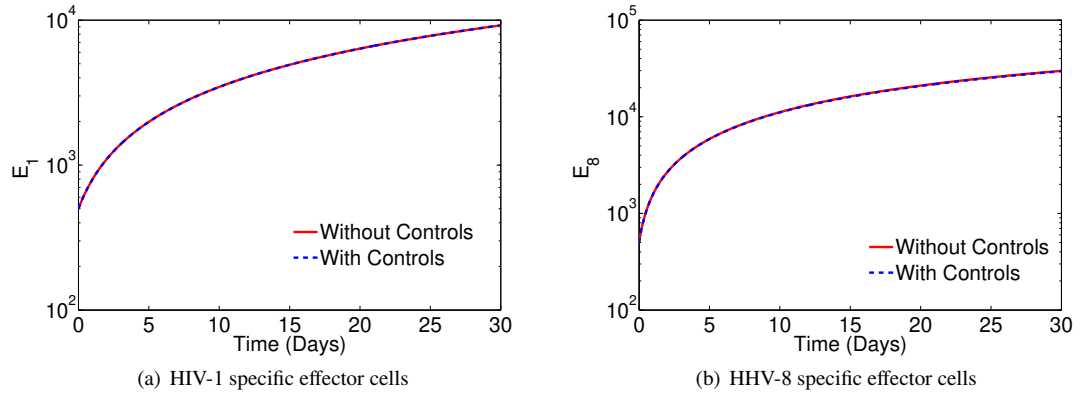(a) HIV-1 specific effector cells

(b) HHV-8 specific effector cells

Figure 11: Effector cells with and without controls.

bound in the drug level till day 6 and 18, respectively before gradually declining to the final time. The control ζ_p is at minimum dosage before rising to its upper bound, a level it maintains until the end of the intervention.
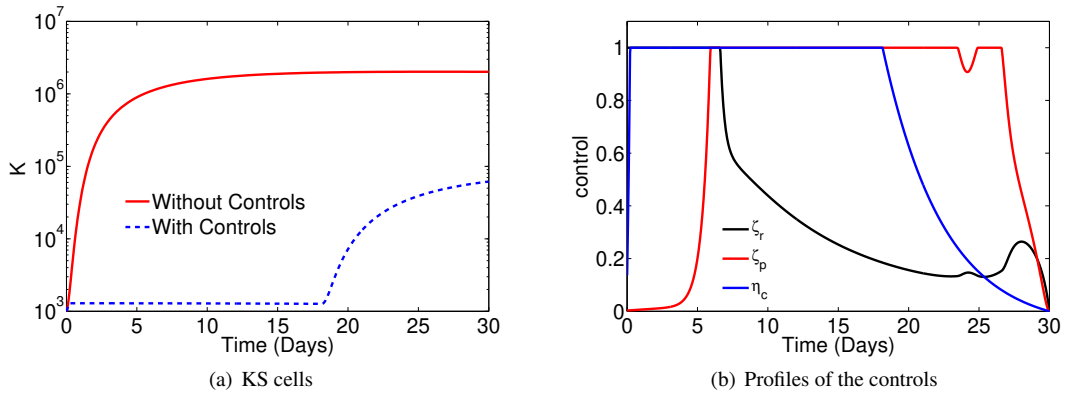

(a) KS cells

(b) Profiles of the controls

Figure 12: KS with and without control and the control profiles.

8. Conclusion

AIDS-KS continues to be diagnosed in HIV infected patients despite the introduction of HAART. This is an indication that the first-line and second-line antiretroviral regimens as recommended by WHO might not work for all patients to prevent HIV-1 related infections. In this study we have formulated mathematical models based on viremia levels for both HIV-1 and HHV-8 to study the prognosis of KS and to make recommendations on optimal dosage regimen for HIV-1 that would clear the viral infections (both HIV-1 and HHV-8), prevent tumor growth and minimize drug toxicity.

We have found that for constant infected CD4$^+$ T-cell and B-cell sources (both from infection and proliferation) that is $\gamma = \beta = 0$, both HIV-1 and HHV-8 infections, measured by viral and infected cell levels, decline to below detectable levels. This result is true even for high constant initial infected CD4$^+$ T-cell and B-cell sources (large r_{x_1} and r_{x_4}). For constant infected CD4$^+$ T-cell and B-cell sources the respective effector cells (E_1 and E_8) are able to proliferate to levels that dominate and overcome the viral replenishment.

If the source for infected B-cells is constant ($\gamma = 0$) but the source for infected CD4$^+$ T-cells is strong ($\beta = 1$) then KS fails to develop since the HHV-8 VL which is responsible for KS development declines to below a detectable level even for a high constant initial source of infected B-cells. This is the case describing a scenario when HIV-1 infected individuals never suffer from KS throughout the period of their HIV-1 infection.

When both sources for infected CD4$^+$ T-cells and B-cells are strong ($\gamma = \beta = 1$) both HIV-1 and HHV-8 levels are above their detectable levels, the KS level is also high and the development of clinical KS is possible. This result is true even when the proliferation rates for infected CD4$^+$ T-cells and B-cells r_{x_1} and r_{x_4} are low.

From the three special cases considered above, that is, $\gamma = \beta = 0$, $\gamma = 0$, $\beta = 1$, $\gamma = \beta = 1$ (before controlled treatment is administered) and the other cases $0 < \gamma < 1$ and $0 < \beta < 1$ (not shown in the paper as it is inferred in the special cases), it can be deduced that the success of viral invasion of the host hinges on viral production from variable infected T and B cell sources being continuously variable. The variability of viral production is a necessary condition to ensure that the immune effector cells are unable to mount a sufficient response to overcome the viral replication.

For the strong viral sources $\gamma = 1$, $\beta = 1$ discussed above, we have shown that when treatment control parameters ζ_r, ζ_p and η_c representing efficacies for reverse transcriptase inhibitors, protease inhibitors and chemotherapy, respectively are introduced, it is possible to find optimal treatment levels ζ_r^*, ζ_p^* and η_c^* above which the HIV-1 infection declines to below detectable level resulting in the clearance of HHV-8.

We simulated the case $\gamma = \beta = 1$ above which yielded high VLs and a possibility of clinical KS. The conclusion when $\zeta_r \geq \zeta_r^*$, $\zeta_p \geq \zeta_p^*$, $\eta_c \geq \eta_c^*$, $\gamma = \beta = 1$ yielded a different outcome as in this case the VL for both HIV-1 and HHV-8 declined to undetectable levels for any source of infected CD4$^+$ T-cella and B-cells.

Our work is important in that it supports the recommendation for early treatment for HIV-1 patients as a means to maintain low VLs and to prevent HIV-1 related infections. Our work also informs HIV-1 infected individuals about the importance of adhering to treatment to maintain low VLs as this would help to maintain the same treatment regimens and acceptable toxic levels.

A. Appendix

A.1. Matrix M

Entries from the following matrix **M** from Section 3 is used throughout this paper to abbreviate other matrices:

$$
\mathbf{M} = \begin{pmatrix}
M_{11} & 0 & 0 & 0 & 0 & 0 & M_{17} \\
M_{21} & M_{22} & 0 & 0 & 0 & 0 & 0 \\
0 & 0 & M_{33} & 0 & 0 & M_{36} & 0 \\
0 & 0 & 0 & M_{44} & 0 & M_{46} & 0 \\
0 & 0 & 0 & 0 & M_{55} & 0 & M_{57} \\
0 & 0 & 0 & M_{64} & 0 & M_{66} & 0 \\
M_{71} & 0 & 0 & 0 & 0 & 0 & M_{77}
\end{pmatrix},
$$

where $M_{11} = -\left(\mu_{x_1} + \kappa_1 \dfrac{s_{x_5}}{(\mu_{x_5} - r_{x_5})}\right)$, $M_{17} = r_{x_1}$, $M_{21} = \alpha$, $M_{22} = -\kappa_3 \dfrac{s_{x_5}}{(\mu_{x_5} - r_{x_5})}$, $M_{33} = -(\mu_{x_3} - r_{x3})$,

$M_{36} = r_{x_3} \dfrac{s_{x_3}}{(\mu_{x_3} - r_{x_3})}$, $M_{44} = -\left(\kappa_4 \dfrac{s_{x_3}}{(\mu_{x_3} - r_{x_3})} + \mu_{x_4}\right)$, $M_{46} = r_{x_4}$, $M_{55} = -(\mu_{x_5} - r_{x_5})$, $M_{57} = r_{x_5} \dfrac{s_{x_5}}{(\mu_{x_5} - r_{x_5})}$,

$M_{64} = N_{x_6}\mu_{x_4}$, $M_{66} = -\mu_{x_6}$, $M_{71} = N_{x_7}\mu_{x_1}(1 + \delta)$, $M_{77} = -\mu_{x_7}$.

A.2. Coefficients of the Characteristic Polynomial

These results are for the coefficients of the characteristic polynomial of the $\gamma = \beta = 1$ case for weak viral source model and all cases for the strong viral source model.

$$
a_1 = \left[\left(\mu_{x_1} + \kappa_1 \frac{s_{x_5}}{(\mu_{x_5} - r_{x_5})}\right) + \mu_{x_7}\right] + \left[\left(\kappa_4 \frac{s_{x_3}}{(\mu_{x_5} - r_{x_5})} + \mu_{x_4}\right) + \mu_{x_6}\right] > 0
$$

$$
a_2 = \left\{\left[\frac{\mu_{x_7}}{(\mu_{x_5} - r_{x_5})}(\mu_{x_1}(\mu_{x_5} - r_{x_5}) + \kappa_1 s_{x_5})\right] + \left[\frac{\mu_{x_6}}{(\mu_{x_5} - r_{x_5}) - r_{x_3}}(\kappa_4 s_{x_3} + \mu_{x_4}(\mu_{x_5} - r_{x_5}) - r_{x_3}))\right]\right\}
$$

$$
\times (1 - \mathcal{R}_{0x_i}) + \left[\left(\kappa_4 \frac{s_{x_3}}{(\mu_{x_5} - r_{x_5})} + \mu_{x_4}\right) + \mu_{x_6}\right]\left[\left(\mu_{x_1} + \kappa_1 \frac{s_{x_5}}{(\mu_{x_5} - r_{x_5})}\right) + \mu_{x_7}\right]
$$

$$
> \left\{\left[\frac{\mu_{x_7}}{(\mu_{x_5} - r_{x_5})}(\mu_{x_1}(\mu_{x_5} - r_{x_5}) + \kappa_1 s_{x_5})\right] + \left[\frac{\mu_{x_6}}{(\mu_{x_5} - r_{x_5})}(\kappa_4 s_{x_3} + \mu_{x_4}(\mu_{x_5} - r_{x_5}))\right]\right\} \times (1 - \mathcal{R}_{0x_i}) > 0,
$$

$$
a_3 = \left\{\left[\left(\kappa_4 \frac{s_{x_3}}{(\mu_{x_3} - r_{x_3})} + \mu_{x_4}\right) + \mu_{x_6}\right]\left[\frac{\mu_{x_7}}{(\mu_{x_5} - r_{x_5})}(\mu_{x_1}(\mu_{x_5} - r_{x_5}) + \kappa_1 s_{x_5})\right]\right.
$$

$$
+ \left[\frac{\mu_{x_6}}{(\mu_{x_3} - r_{x_3})}(\kappa_4 s_{x_3} + \mu_{x_4}(\mu_{x_3} - r_{x_3}))\right]\left[\left(\mu_{x_1} + \kappa_1 \frac{s_{x_5}}{(\mu_{x_5} - r_{x_5})}\right) + \mu_{x_7}\right]\right\}(1 - \mathcal{R}_{0x_i}) > 0,
$$

$$
a_4 = \frac{\mu_{x_6}}{(\mu_{x_3} - r_{x_3})}(\kappa_4 s_{x_3} + \mu_{x_4}(\mu_{x_3} - r_{x_3}))\frac{\mu_{x_7}}{(\mu_{x_5} - r_{x_5})}(\mu_{x_1}(\mu_{x_5} - r_{x_5}) + \kappa_1 s_{x_5})(1 - \mathcal{R}_{0x_i})^2 > 0.
$$

since all parameters are positive.

A.3. Proof of Local Stability when $\gamma = \beta = 1$ for the Weak Viral Source Model

We are going to show that $a_1 a_2 a_3 - a_3^2 - a_1^2 a_4 > 0$. Hence, we have

$$
a_1 a_2 a_3 - a_3^2 - a_1^2 a_4 =
$$

$$
\left[\left(\mu_{x_1} + \kappa_1 \frac{s_{x_5}}{(\mu_{x_5} - r_{x_5})}\right) + \mu_{x_7}\right]\left[\frac{\mu_{x_7}}{(\mu_{x_5} - r_{x_5})}(\mu_{x_1}(\mu_{x_5} - r_{x_5}) + \kappa_1 s_{x_5})(1 - \mathcal{R}_{0x_7})\right]
$$

$$
\times \left[\left(\kappa_4 \frac{s_{x_3}}{(\mu_{x_3} - r_{x_3})} + \mu_{x_4}\right) + \mu_{x_6}\right]\left[\frac{\mu_{x_7}}{(\mu_{x_5} - r_{x_5})}(\mu_{x_1}(\mu_{x_5} - r_{x_5}) + \kappa_1 s_{x_5})(1 - \mathcal{R}_{0x_7})\right]
$$

$$
+ \left[\left(\mu_{x_1} + \kappa_1 \frac{s_{x_5}}{(\mu_{x_5} - r_{x_5})}\right) + \mu_{x_7}\right]\left[\left(\kappa_4 \frac{s_{x_3}}{(\mu_{x_3} - r_{x_3})} + \mu_{x_4}\right) + \mu_{x_6}\right]\left[\left(\mu_{x_1} + \kappa_1 \frac{s_{x_5}}{(\mu_{x_5} - r_{x_5})}\right) + \mu_{x_7}\right]
$$

$$\times \left[\frac{\mu_{x_6}}{(\mu_{x_3} - r_{x_3})}(\kappa_4 s_{x_3} + \mu_{x_4}(\mu_{x_3} - r_{x_3}))(1 - \mathcal{R}_{0x_6}) \right] \left[\left(\mu_{x_1} + \kappa_1 \frac{s_{x_5}}{(\mu_{x_5} - r_{x_5})} \right) + \mu_{x_7} \right]$$

$$+ \left[\left(\kappa_4 \frac{s_{x_3}}{(\mu_{x_3} - r_{x_3})} + \mu_{x_4} \right) + \mu_{x_6} \right] \left[\left(\kappa_4 \frac{s_{x_3}}{(\mu_{x_3} - r_{x_3})} + \mu_{x_4} \right) + \mu_{x_6} \right] \left[\left(\mu_{x_1} + \kappa_1 \frac{s_{x_5}}{(\mu_{x_5} - r_{x_5})} \right) + \mu_{x_7} \right]$$

$$\times \left[\left(\kappa_4 \frac{s_{x_3}}{(\mu_{x_3} - r_{x_3})} + \mu_{x_4} \right) + \mu_{x_6} \right] \left[\frac{\mu_{x_7}}{(\mu_{x_5} - r_{x_5})}(\mu_{x_1}(\mu_{x_5} - r_{x_5}) + \kappa_1 s_{x_5})(1 - \mathcal{R}_{0x_7}) \right]$$

$$+ \left[\left(\kappa_4 \frac{s_{x_3}}{(\mu_{x_3} - r_{x_3})} + \mu_{x_4} \right) + \mu_{x_6} \right] \left[\frac{\mu_{x_6}}{(\mu_{x_3} - r_{x_3})}(\kappa_4 s_{x_3} + \mu_{x_4}(\mu_{x_3} - r_{x_3}))(1 - \mathcal{R}_{0x_6}) \right]$$

$$\times \left[\frac{\mu_{x_6}}{(\mu_{x_3} - r_{x_3})}(\kappa_4 s_{x_3} + \mu_{x_4}(\mu_{x_3} - r_{x_3}))(1 - \mathcal{R}_{0x_6}) \right] \left[\left(\mu_{x_1} + \kappa_1 \frac{s_{x_5}}{(\mu_{x_5} - r_{x_5})} \right) + \mu_{x_7} \right]$$

$$+ \left[\left(\kappa_4 \frac{s_{x_3}}{(\mu_{x_3} - r_{x_3})} + \mu_{x_4} \right) + \mu_{x_6} \right] \left[\left(\kappa_4 \frac{s_{x_3}}{(\mu_{x_3} - r_{x_3})} + \mu_{x_4} \right) + \mu_{x_6} \right] \left[\left(\mu_{x_1} + \kappa_1 \frac{s_{x_5}}{(\mu_{x_5} - r_{x_5})} \right) + \mu_{x_7} \right]$$

$$\times \left[\frac{\mu_{x_6}}{(\mu_{x_3} - r_{x_3})}(\kappa_4 s_{x_3} + \mu_{x_4}(\mu_{x_3} - r_{x_3}))(1 - \mathcal{R}_{0x_6}) \right] \left[\left(\mu_{x_1} + \kappa_1 \frac{s_{x_5}}{(\mu_{x_5} - r_{x_5})} \right) + \mu_{x_7} \right]$$

$$+ \left[\left(\mu_{x_1} + \kappa_1 \frac{s_{x_5}}{(\mu_{x_5} - r_{x_5})} \right) + \mu_{x_7} \right] \left[\left(\kappa_4 \frac{s_{x_3}}{(\mu_{x_3} - r_{x_3})} + \mu_{x_4} \right) + \mu_{x_6} \right]$$

$$\times \left[\frac{\mu_{x_7}}{(\mu_{x_5} - r_{x_5})}(\mu_{x_1}(\mu_{x_5} - r_{x_5}) + \kappa_1 s_{x_5})(1 - \mathcal{R}_{0x_7}) \right]$$

$$\times \left\{ \left[\left(\mu_{x_1} + \kappa_1 \frac{s_{x_5}}{(\mu_{x_5} - r_{x_5})} \right) + \mu_{x_7} \right] \left[\left(\kappa_4 \frac{s_{x_3}}{(\mu_{x_3} - r_{x_3})} + \mu_{x_4} \right) + \mu_{x_6} \right] \right.$$

$$\left. - 2\frac{\mu_{x_6}}{(\mu_{x_3} - r_{x_3})}(\kappa_4 s_{x_3} + \mu_{x_4}(\mu_{x_3} - r_{x_3}))(1 - \mathcal{R}_{0x_6}) \right\}$$

It suffices to show that

$$\left[(\mu_{x_1} + \kappa_1 \frac{s_{x_5}}{(\mu_{x_5} - r_{x_5})}) + \mu_{x_7} \right] \left[\left(\kappa_4 \frac{s_{x_3}}{(\mu_{x_3} - r_{x_3})} + \mu_{x_4} \right) + \mu_{x_6} \right]$$

$$- 2\frac{\mu_{x_6}}{(\mu_{x_3} - r_{x_3})}(\kappa_4 s_{x_3} + \mu_{x_4}(\mu_{x_3} - r_{x_3}))(1 - \mathcal{R}_{0x_6}) > 0$$

Now,

$$\left[\left(\mu_{x_1} + \kappa_1 \frac{s_{x_5}}{(\mu_{x_5} - r_{x_5})} \right) + \mu_{x_7} \right] \left[\left(\kappa_4 \frac{s_{x_3}}{(\mu_{x_3} - r_{x_3})} + \mu_{x_4} \right) + \mu_{x_6} \right]$$

$$- 2\frac{\mu_{x_6}}{(\mu_{x_3} - r_{x_3})}(\kappa_4 s_{x_3} + \mu_{x_4}(\mu_{x_3} - r_{x_3}))(1 - \mathcal{R}_{0x_6})$$

$$= \frac{1}{(\mu_{x_5} - r_{x_5})} \left[(\mu_{x_1}(\mu_{x_5} - r_{x_5}) + \kappa_1 s_{x_5}) + \mu_{x_7}(\mu_{x_5} - r_{x_5}) \right]$$

$$\times \frac{1}{(\mu_{x_3} - r_{x_3})} \left[(\kappa_4 s_{x_3} + \mu_{x_4}(\mu_{x_3} - r_{x_3})) + \mu_{x_6}(\mu_{x_3} - r_{x_3}) \right] - 2\frac{\mu_{x_6}}{(\mu_{x_3} - r_{x_3})}(\kappa_4 s_{x_3} + \mu_{x_4}(\mu_{x_3} - r_{x_3}))(1 - \mathcal{R}_{0x_6})$$

$$= \frac{1}{(\mu_{x_3} - r_{x_3})(\mu_{x_5} - r_{x_5})} \left[\mu_{x_1}(\mu_{x_5} - r_{x_5}) + \kappa_1 s_{x_5} + \mu_{x_7}(\mu_{x_5} - r_{x_5}) \right] \left[\kappa_4 s_{x_3} + \mu_{x_4}(\mu_{x_3} - r_{x_3}) + \mu_{x_6}(\mu_{x_3} - r_{x_3}) \right]$$

$$- 2\frac{\mu_{x_6}}{(\mu_{x_3} - r_{x_3})}(\kappa_4 s_{x_3} + \mu_{x_4}(\mu_{x_3} - r_{x_3}))(1 - \mathcal{R}_{0x_6})$$

$$= \frac{1}{(\mu_{x_3} - r_{x_3})(\mu_{x_5} - r_{x_5})} \left[\mu_{x_1}(\mu_{x_5} - r_{x_5}) + \kappa_1 s_{x_5} + \mu_{x_7}(\mu_{x_5} - r_{x_5}) \right] \left[\kappa_4 s_{x_3} + \mu_{x_4}(\mu_{x_3} - r_{x_3}) + \mu_{x_6}(\mu_{x_3} - r_{x_3}) \right]$$

$$- \frac{2}{(\mu_{x_3} - r_{x_3})(\mu_{x_5} - r_{x_5})} (\kappa_4 s_{x_3}(\mu_{x_5} - r_{x_5})\mu_{x_6} + \mu_{x_4}(\mu_{x_3} - r_{x_3})(\mu_{x_5} - r_{x_5})\mu_{x_6})(1 - \mathcal{R}_{0x_6})$$

$$= \left[\mu_{x_1}(\mu_{x_5} - r_{x_5}) + \kappa_1 s_{x_5} + \mu_{x_7}(\mu_{x_5} - r_{x_5})\right]\left[\kappa_4 s_{x_3} + \mu_{x_4}(\mu_{x_3} - r_{x_3}) + \mu_{x_6}(\mu_{x_3} - r_{x_3})\right]$$

$$- 2(\kappa_4 s_{x_3}(\mu_{x_5} - r_{x_5})\mu_{x_6} + \mu_{x_4}(\mu_{x_3} - r_{x_3})(\mu_{x_5} - r_{x_5})\mu_{x_6})(1 - \mathcal{R}_{0x_6})$$

$$= \kappa_4 s_{x_3}\mu_{x_1}(\mu_{x_5} - r_{x_5}) + \mu_{x_4}(\mu_{x_3} - r_{x_3})\mu_{x_1}(\mu_{x_5} - r_{x_5}) + \mu_{x_6}(\mu_{x_3} - r_{x_3})\mu_{x_1}(\mu_{x_5} - r_{x_5}) + \kappa_4 s_{x_3}\kappa_1 s_{x_5}$$

$$+ \mu_{x_4}(\mu_{x_3} - r_{x_3})\kappa_1 s_{x_5} + \mu_{x_6}(\mu_{x_3} - r_{x_3})\kappa_1 s_{x_5} + \kappa_4 s_{x_3}\mu_{x_7}(\mu_{x_5} - r_{x_5}) + \mu_{x_4}(\mu_{x_3} - r_{x_3})\mu_{x_7}(\mu_{x_5} - r_{x_5})$$

$$+ \mu_{x_6}(\mu_{x_3} - r_{x_3})\mu_{x_7}(\mu_{x_5} - r_{x_5}) - (2\kappa_4 s_{x_3}(\mu_{x_5} - r_{x_5})\mu_{x_6} + 2\mu_{x_4}(\mu_{x_3} - r_{x_3})(\mu_{x_5} - r_{x_5})\mu_{x_6})(1 - \mathcal{R}_{0x_6})$$

We can show that for $\mathcal{R}_{0x_6} < 1$ the following holds

$$\kappa_4 s_{x_3}\mu_{x_1}(\mu_{x_5} - r_{x_5}) + \mu_{x_4}(\mu_{x_3} - r_{x_3})\mu_{x_1}(\mu_{x_5} - r_{x_5}) + \mu_{x_6}(\mu_{x_3} - r_{x_3})\mu_{x_1}(\mu_{x_5} - r_{x_5}) + \kappa_4 s_{x_3}\kappa_1 s_{x_5}$$

$$+ \mu_{x_4}(\mu_{x_3} - r_{x_3})\kappa_1 s_{x_5} + \mu_{x_6}(\mu_{x_3} - r_{x_3})\kappa_1 s_{x_5} + \kappa_4 s_{x_3}\mu_{x_7}(\mu_{x_5} - r_{x_5}) + \mu_{x_4}(\mu_{x_3} - r_{x_3})\mu_{x_7}(\mu_{x_5} - r_{x_5})$$

$$+ \mu_{x_6}(\mu_{x_3} - r_{x_3})\mu_{x_7}(\mu_{x_5} - r_{x_5}) - 2\kappa_4 s_{x_3}(\mu_{x_5} - r_{x_5})\mu_{x_6} - 2\mu_{x_4}(\mu_{x_3} - r_{x_3})(\mu_{x_5} - r_{x_5})\mu_{x_6} > 0$$

$$\implies \kappa_4 s_{x_3}(\mu_{x_5} - r_{x_5})(\mu_{x_1} - 2\mu_{x_6}) + \mu_{x_4}(\mu_{x_3} - r_{x_3})(\mu_{x_5} - r_{x_5})(\mu_{x_1} - 2\mu_{x_6}) > 0$$

$$\implies \mu_{x_1} - 2\mu_{x_6} > 0 \implies \frac{\mu_{x_1}}{\mu_{x_6}} > 2$$

Hence, $a_1 a_2 a_3 - a_3^2 - a_1^2 a_4 > 0$ on condition that $\frac{\mu_{x_1}}{\mu_{x_6}} > 2$.

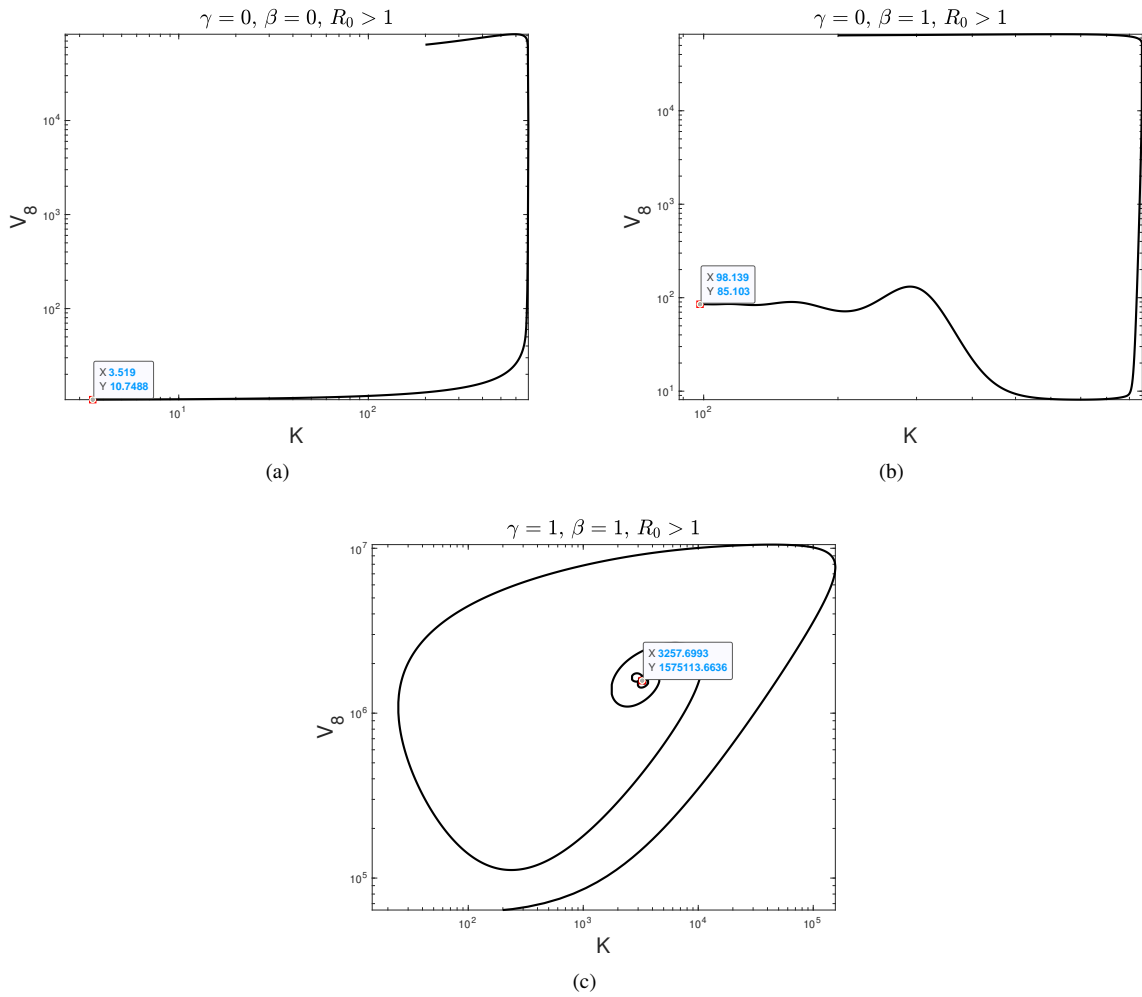## A.4. Contour Plots for the Weak and Strong Viral Source Model

(a)

(b)

(c)

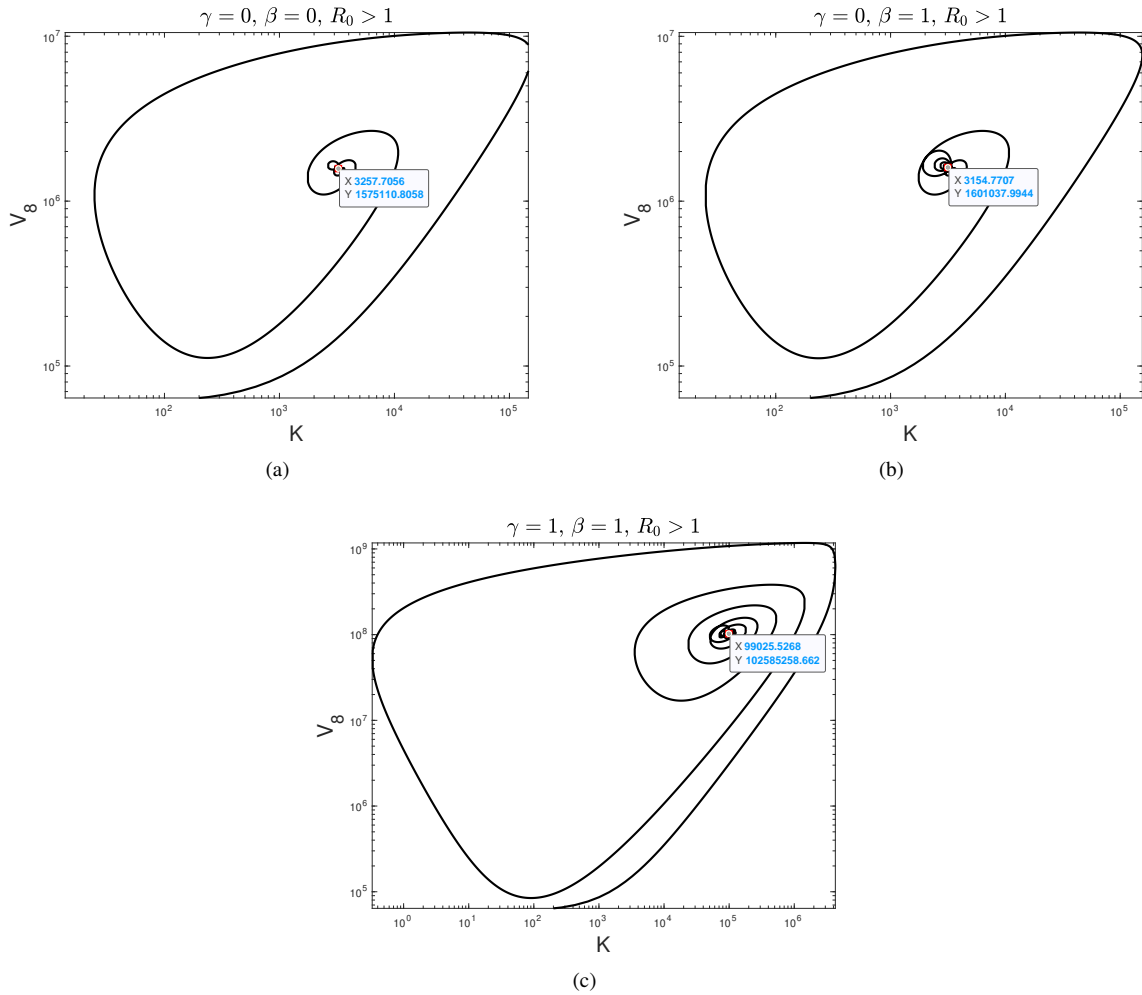**Figure 13:** Contour plots for weak viral source model.

Figure 14: Contour plots for strong viral source model.

References

[1] Bajaria, S., Kirschner, D., 2005. CTL action during HIV-1 is determined via interactions with multiple cell types. World Sientific, Singapore and New Jersey.

[2] Benjamini, Y., Hochberg, Y., 1995. Controlling the false discovery rate: A practical and powerful approach to multiple testing. Journal of the Royal Statistical Society. Series B (Methodological) 57(1), 289–300.

[3] Blower, S.M., Dowlatabadi, H., 1994. Sensitivity and uncertainty analysis of complex models of disease transmission: An HIV model, as an example. International Statistical Review / Revue Internationale de Statistique 62(2), 229–243.

[4] Boer, R.D., Ribeiro, R.M., Perelson, A.S., 2010. Current estimates for HIV-1 production imply rapid viral clearance in lymphoid tissues. PLoS Comput Biol 6(9), e1000906.

[5] Castillo-Chavez, C., Feng, Z., Huang, W., 2002. On the computation of R_0 and its role in global stability. Institute for Mathematics and Its Applications 125, 229.

[6] Chang, Y., Cesarman, E., S., P.M., Lee, F., Culpepper, J., Knowles, D., Moore, P.S., 1994. Identification of herpesvirus-like DNA sequences in AIDS-associated Kaposi's sarcoma. Science 266, 14–15.

[7] Cheung, M.C., Pantanowitz, L., Dezube, B.J., 2005. AIDS-related malignancies: Emerging challenges in the era of highly active antiretroviral therapy. The Oncologist 10, 412–426.

[8] Chiereghin, A., Barozzi, P., Petrisli, E., Piccirilli, G., Gabrielli, L., Riva, G., Potenza, L., Cappelli, G., Ruvo, N.D., Libri, I., Maggiore, U., Morelli, M.C., Potena, L., Todeschini, P., Gibertoni, D., Labanti, M., Sangiorgi, G., Manna, G.L., Pinna, A.D., Luppi, M., Lazzarotto, T., 2017. Multicenter prospective study for laboratory diagnosis of HHV8 infection in solid organ donors and transplant recipients and evaluation of the clinical impact after transplantation. Transplantation 101(8), 1935–1944.

[9] Cho, B.K., Rao, V.P., Ge, Q., Eisen, H.N., Chen, J., 2000. Homeostasis-stimulated proliferation drives naive T cells to differentiate directly into memory t cells. J. Exp. Med 192(4, 549–556.

[10] Dittmer, D.P., L.Richards, K., Damania, B., 2012. Treatment of Kaposi sarcoma associated herpesvirus associated cancers. Frontiers in Microbiology 3, 141.

[11] Fieller, E.C., Hartley, H.O., Pearson, E.S., 1957. Tests for rank correlation coefficients. I. Biometrika 44, 480–481.

[12] Foglieni, C., Scabini, S., Belloni, D., Broccolo, F., Lusso, P., Malnati, M., Ferrero, E., 2005. Productive infection of HUVEC by HHV-8 is associated with changes compatible with angiogenic transformation. European Journal of Histochemistry 49(3), 273–284.

[13] Foreman, K., 2001. Kaposi's sarcoma: The role of HHV-8 and HIV-1 in pathogenesis. Expert Reviews in Molecular Medicine 3(9), 1–7.

[14] Gbabe, O., Okwundu, C., Dedicoat, M., Freeman, E., 2014. Treatment of severe or progressive Kaposi's sarcoma in HIV-infected adults. Cochrane Database of Systematic Reviews 9, 1–7.

[15] Glass, T., Myer, L., Lesosky, M., 2020. The role of HIV viral load in mathematical models of HIV transmission and treatment: a review. BMJ Global Health 5::e001800.

[16] Gomero, B., 2012. Latin Hypercube Sampling and Partial Rank Correlation Coefficient Analysis Applied to an Optimal Control Problem. Master's thesis. University of Tennessee. Knoxvill.

[17] Guiota, C., Delsantob, P., A.Carpinterid, Pugnod, N., Mansurye, Y., Deisboecke, T., 2006. The dynamic evolution of the power exponent in a universal growth model of tumors. Journal of Theoretical Biology 240, 459–463.

[18] Gumel, A., Zhang, X., Shivakumar, P., Garba, M., Sahai, B., 2002. A new mathematical model for assessing therapeutic strategies for HIV infection. Journal of Theoretical Medicine 4(2), 147–155.

[19] Hadinoto, V., Shapiro, M., Sun, C.C., Thorley-Lawson, D.A., 2009. The dynamics of EBV shedding implicate a central role for epithelial cells in amplifying viral output. PLoS Pathog 5(7), e1000496.

[20] Hockett, R.D., Kilby, J.M., Derdeyn, C.A., Saag, M.S., Sillers, M., Squires, K., Chiz, S., Nowak, M.A., Shaw, G.M., Bucy, R.P., 1999. Constant mean viral copy number per infected cell in tissues regardless of high, low, or undetectable plasma HIV RNA. Journal of Experimental Medicine 189, 1545–1554.

[21] Holash, J., Davis, S., Papadopoulos, N., Croll, S.D., Ho, L., Russell, M., Boland, P., Leidich, R., Hylton, D., Burova, E., Ioffe, E., Huang, T., Radziejewski, C., Bailey, K., Fandl, J.P., Daly, T., Wiegand, S.J., Yancopoulos, G.D., Rudge, J.S., 2002. VEGF-Trap: A VEGF blocker with potent antitumor effects. Proc Natl Acad Sci U S A. 99(17), 99(17): 11393–11398.

[22] Huynh, G., Adler, F., 2012. Mathematical modelling the age dependence of Epstein-Barr virus associated infectious mononucleosis. Mathematical Medicine and Biology : a Journal of the IMA 29(3), 245–61.

[23] Institute, N.C., 2011. HIV infection and cancer risk. URL: http://www.cancer.gov/cancertopics/factsheet/Risk/hiv-infection.

[24] Kirschner, D., Lenhart, S., Serbin, S., 1997. Optimal control of the chemotherapy of HIV. J. Math. Biol. 35, 775–792.

[25] Louzoun, Y., Xue, C., Lesinski, G., A.Friedman, 2014. A mathematical model for pancreatic cancer growth and treatments. Journal of Theoretical Biology 351, 74–82.

[26] Lungu, E., Massaro, T.J., Ndelwa, E., Ainea, N., Chibaya, S., J.Malunguza, N., 2013. Mathematical modelling of the HIV Kaposi's sarcoma coinfection dynamics in areas of high HIV prevalence. Computational and Mathematical Methods in Medicine 2013, 12.

[27] Marino, S., Hogue, I., Ray, C., Kirschner, D., 2008. A methodology for performing global uncertainty and sensitivity analysis in systems biology. Journal of Theoretical Biology 254(1), 198–196.

[28] Mclean, A.R., Michie, C.A., 1995. In vivo estimates of division and death rates of human T lymphocytes. Immunology 92, 3707–3711.

[29] Nachega, J.B., Marconi, V.C., van Zyl, G.U., Gardner, E.M., Preiser, W., Hong, S.Y., Mills, E., Gross, R., 2011. HIV treatment adherence, drug resistance, virologic failure: Evolving concepts. Infect Disord Drug Targets 11(2), 167–174.

[30] Nani, F., Jin, M., 2011. Dynamics of HIV-1 associated Kaposi sarcoma during haart therapy. International Conference on Bioinformatics and Computational Biology 11, 783–786.

[31] Nani, F., Jin, M., 2016. Analysis of dynamics of HIV-1 associated Kaposi sarcoma during HAART and ACI. British Journal of Mathematics and Computer Science 19(1), 1–22.

[32] World Health Organisation, 2016. Consolidated guidelines on the use of antiretroviral drugs for treating and preventing HIV infection: recommendations for a public health approach. World Health Organisation, Switzerland.

[33] Organisation, W.H., 2010. Adherence to longterm therapies: Evidence for action. URL: http://www.who.int/chp/knowledge/publications/adherence_report/en/.

[34] Organisation, W.H., 2017. What's new in treatment monitoring: Viral load and CD4 testing. URL: http://www.who.int/hiv.

[35] Perelson, A., 2002. Modelling viral and immune system dynamics. Nature Reviews 2, 28–36.

[36] Perelson, A., Nelson, P., 1999. Mathematical analysis of HIV-1: Dynamics in vivo. Society for Industrial and Applied Mathematics 41, 3–44.

[37] Pillis, L.D., Gu, W., Fister, K.R., Head, T., Maples, K., Murugan, A., Neal, T., Yoshida, K., 2007. Chemotherapy for tumors: An analysis of the dynamics and a study of quadratic and linear optimal controls. Math. Biosci. 209, 292–315.

[38] Purushothaman, P., Uppal, T., Verma, S.C., 2015. Molecular biology of KSHV lytic reactivation. Viruses 7, 116–153.

[39] Shapiro, M., Duca, K., Lee, K., Delgado-Eckert, E., Hawkins, J., Jarrah, A., Laubenbacher, R., Polys, N., Hadinoto, V., Thorley-Lawson, D., 2008. A virtual look at Epstein–Barr virus infection: Simulation mechanism. Journal of Theoretical Biology 252(4), 633–648.

[40] Shoko, C., Chikobvu, D., 2019. A superiority of viral load over CD4 cell count when predicting mortality in HIV patients on therapy. BMC Infectious Diseases 19:169.

[41] S.Lenhart, Workman, J.T., 2007. Optimal Control Applied to Biological Models. CRC Press, Taylor and Francis Group, London.

[42] Stilianakis, N., Schenzle, D., 2005. On the intra-host dynamics of HIV-1 infections. Mathematical Biosciences 199(2006), 1–25.

[43] Support, M.C., 2016. About kaposi's sarcoma. URL: http://www.macmillan.org.uk.

[44] Szomolay, B., Lungu, E., 2014. A mathematical model for the treatment of AIDS-related Kaposi's sarcoma. Journal of Biological Systems 22, 495–522.

[45] Turner, B.J., 2002. Adherence to antiretroviral therapy by human immunodeficiency virus–infected patients. The Journal of Infectious Diseases 185(2, S143–51.

[46] Uldrick, S., Whitby, D., 2011. Update on KSHV-epidemiology, kaposi sarcoma pathogenesis and treatment of Kaposi sarcoma. Cancer Lett. 305(2), 150–162.

[47] UNAIDS, 2019. Global HIV and AIDS statistics — 2019 fact sheet. URL: `https://www.unaids.org/en/resources/fact-sheet`.

[48] Verma, M., Erwin, S., Abedi, V., Hontecillas, R., Hoops, S., Leber, A., Bassaganya-Riera, J., Ciupe, S., 2017. Modeling the mechanisms by which HIV-associated immunosuppression influences HPV persistence at the oral mucosa. PLoS ONE 12(1), e0168133.

[49] West, G., Brown, J., Enquist, B., 2001. A general model for ontogenetic growth. Nature 413, 628–631.

[50] Weston, R., Marett, B., 2009. HIV infection pathology and disease progression. Clinical Pharmacist 1, 387–392.

[51] Zhang, T., Shao, X., Chen, Y., Zhang, T., Minhas, V., Wood, C., He, N., 2012. Human herpesvirus 8 seroprevalence, china. Emerg. Infect. Dis 18, 150–152.